

## 7

# DYNAMIC STEREOCHEMISTRY AND CHIROPTICAL SPECTROSCOPY OF METALLO-ORGANIC COMPOUNDS

James W. Canary and Zhaohua Dai

## 7.1. INTRODUCTION

This chapter aims to give a current overview of the dynamic stereochemistry of metal-based molecular switches together with the role that chiroptical spectroscopy has played in the development of the field. Recent interest and the development of chiroptical spectroscopy tools have led to many exciting discoveries in the dynamic stereochemistry of metal-based chiroptical switches. These materials generally involve a scaffold built upon a metal-chelate complex that is capable of changing its interaction with polarized light upon exposure to an external stimulus. Such molecular switches could play a key role in the development of future optical displays, molecular electronics, and telecommunications materials.

Many metal-based chiroptical switches have been synthesized within the past decade [1–6]. Most of these systems include a transition metal chelated to multiple atoms of an associated chiral ligand. The conformational state of the chelation complex is altered by a multitude of triggering agents such as photochemical irradiation, reducing–oxidizing agents, counterion exchange, and others. Regardless of which trigger is used, the interconversion between states must be efficient, selective, and reversible. The mechanism may involve structural changes induced by the metal ion directly, such as in redox-triggered molecular switches, or the metal may play a structural role or participate in generation of the readout signal.

The means of analysis of these metal-based chiroptical switches is also critical. A nondestructive read-out of the optically active system must be employed in order to gain accurate information about the different states of the switch. Thus, the tools used to accurately assess switching may be limited. Indeed, the presence of the metal may offer limitations on read-out, such as quenching fluorescence of the organic ligand, or may offer new opportunities such as presenting additional chromophoric elements that can be monitored.

*Comprehensive Chiroptical Spectroscopy, Volume 2: Applications in Stereochemical Analysis of Synthetic Compounds, Natural Products, and Biomolecules*, First Edition. Edited by N. Berova, P. L. Polavarapu, K. Nakanishi, and R. W. Woody.  
© 2012 John Wiley & Sons, Inc. Published 2012 by John Wiley & Sons, Inc.

Chiroptical spectroscopic measurements are powerful tools for the characterization of materials in this field [6]. All chiroptical methods are based on the different interaction between an optically active compound and the left- and right-circularly polarized vector components of plane polarized, monochromatic light. These components interact with a chiral medium in two ways: (a) Difference in velocity through the medium results in a circular birefringence or anisotropic refraction ( $n_L - n_R \neq 0$ ), which is observed as a rotation of the plane of polarization. (b) Difference in absorption by the medium results in a circular dichroic effect or anisotropic absorption ( $A_L - A_R \neq 0$ , or  $\Delta\epsilon \neq 0$ ). Anisotropic refraction has been utilized in polarimetry for the determination of optical rotation at a specific wavelength [7]. The rotatory power of a substance varies with the wavelength. The need to measure the optical rotation at different wavelengths led to instruments for recording the optical rotatory dispersion (ORD) over the UV–vis range, which gives information about the change in sign of the rotation on passage of the absorption band, the Cotton effect (CE).

More recently, ORD has largely been replaced by electronic circular dichroism as an experimental technique. Circular dichroism (CD) is the most commonly used method due to the relatively strong information content of this technique as compared, for example, to single-wavelength optical rotation measurement and the widespread availability of sensitive CD instruments. Optical activity is strongly dependent on conformational equilibria, and, therefore, CD and ORD spectroscopy are two techniques that can give telling information on the spatial arrangement of molecules *in solution*. Various mechanisms may give rise to CD, including induced (ICD) and CD exciton chirality. A typical CD spectrum will appear similar to the corresponding UV–vis absorbance spectrum, with amplitude that depends on the strength of the electronic absorbance, the asymmetric distribution of electrons in the molecule, and the coupling between these two phenomena. This typical spectroscopy involving electronic transitions is generally called electronic circular dichroism (ECD), which includes electronic near infrared CD (NIR CD). Vibrational circular dichroism (VCD) and near-infrared vibrational circular dichroism (NIR VCD), which involve vibration transitions, have recently received considerable attention [8–15].

Unless the spectrum can be calculated explicitly, the features of an induced CD spectrum are difficult to interpret on the basis of structural changes other than by comparing to similar systems. An exception is CD exciton chirality, which is particularly useful for solution studies [6, 16] and is covered extensively elsewhere in this volume. Few other spectroscopic signals report structural aspects of molecular conformation or intermolecular association so dramatically. By this feature, CD exciton chirality has been used as a sensitive probe of changes in molecular conformation or intermolecular association.

If the metal-based chiroptical switch is fluorescent, it can be investigated by fluorescence-detected circular dichroism (FDCD) or circularly polarized fluorescence excitation (CPE) [17], which is based on detection in emission, while conventional CD measures the intensity of transmitted light. Such metal-based switches can also be studied by circular polarized luminescence (CPL), which is an emission analogue of circular dichroism and probes chirality of electronically excited species [18].

The character of the chiroptical signal is only one aspect of chiroptical switches. In general, requirements for the design of an efficient metal-based chiroptical molecular switch include: (i) stability of the optically active forms, (ii) chemical reversibility of the switching processes, (iii) high sensitivity of the chiroptical response, and (iv) potential application in multimode switching. There are many systems that achieve these aims. This chapter will be organized by the chiroptical responses of metal-base dynamic stereochemical systems: optical rotation/ORD, ECD, VCD, FDCD/CPE, and CPL. Since

the majority of the systems have been studied mainly by ECD, such systems will be suborganized by input mechanism: First, we will discuss selected examples of metal association and dissociation, which is a seemingly trivial means of triggering chiroptical response but for which several unique and interesting examples will be discussed. Changes in the environment of metallo-organic complexes including solvent, temperature, counterion, and pressure will be discussed. We will mention briefly the Pfeiffer effect, a classic phenomenon that was not originally intended as a chiroptical switch yet involves chemistry that is highly relevant to metal-based chiroptical switches. Redox chemistry is particularly suited to metal-based systems, and therefore redox-triggered chiroptical molecular switches will be discussed at length. Fewer examples of optically induced metal-based chiroptical switches have been reported, and these will also be presented.

Dynamic stereochemistry in the solid state will also be discussed. CD has more often been used to obtain stereochemical information from solutions, while its utility has so far remained limited in the solid state or aggregates. Methods for obtaining solid-state spectra are currently under development, but interpretation of CD data obtained from oriented media is very challenging and subject to error [19]. We will present examples of metal-based chiroptical switches in solid state, although their CD spectra might have been obtained in solution or in polycrystalline form.

## 7.2. METAL-BINDING INDUCED SWITCHES STUDIED BY OPTICAL ROTATION AND ORD

As mentioned, optical rotation and ORD were available much earlier than other forms of chiroptical spectroscopy. In the absence of modern computational methods, limited structural conclusions were available from such data. However, very remarkable chemistry related to metal-based chiroptical switches was examined using these techniques. Several examples will be discussed here.

### 7.2.1. Foundational Studies: Octahedral Complexes of Transition Metals

The ability to turn “off” a chiroptical signal by changing the environment was known from the earliest days of coordination chemistry and established by monitoring optical rotation. One of the two enantiomers of  $\text{Co(en)}_3^{3+}$  (where  $\text{en} = \text{NH}_2\text{CH}_2\text{CH}_2\text{NH}_2$ ) that Werner [20] resolved in 1912 rotates plane polarized light from the sodium D line (589.3 nm) toward the right while the other rotates the light by the same amount in the opposite direction. Plotting the values of  $[\alpha]_\lambda$  of  $\Lambda(+)\text{Co(en)}_3^{3+}$  as a function of wavelength results in its ORD curve. Since the resolved enantiomer of  $\text{Co(en)}_3^{3+}$  may be racemized by boiling an aqueous solution of one of the enantiomers in the presence of activated charcoal, this dynamic stereochemistry was originally monitored by optical rotation or ORD. In this context, it should be mentioned that ORD and ECD are not truly independent methods [21] and theoretical ORD and ECD spectra can be obtained in a single quantum mechanical calculation [22]. Thus, in a sense, the ability to trigger “off” a metal-based switched was known from the beginning of coordination chemistry in part because optical rotation was available at this early time as a technique that could report the racemization reaction.

### 7.2.2. Metal-Based Chiroptical Switches Controlled by Polarized Light

Optical rotation was used to show that partial optical resolution can be achieved by enriching one enantiomer when irradiating a racemic mixture with right- or left-circularly polarized light. This phenomenon is the consequence of differential absorptivity of circularly polarized light by enantiomers, resulting in the preferential isomerization of one enantiomer over the other. Yoneda et al. [23] used an argon ion laser to partially photoresolve tris(acetylacetonato)chromium (III) ( $\text{Cr}(\text{acac})_3$ ) and related complexes. Linearly polarized light emitted from the laser was passed through a quarter-waveplate matched for the 514.5 nm wavelength of the laser to produce circularly polarized light. This process was monitored by following optical rotation of the sample as a function of time (Figure 7.1). At time  $t = 100$  min, the sense of the circularly polarized light was inverted by rotating the quarter-waveplate  $90^\circ$ . The data clearly show that the photoresolution process is switchable. A 4.8% resolution was achieved and no measurable photodecomposition occurred.

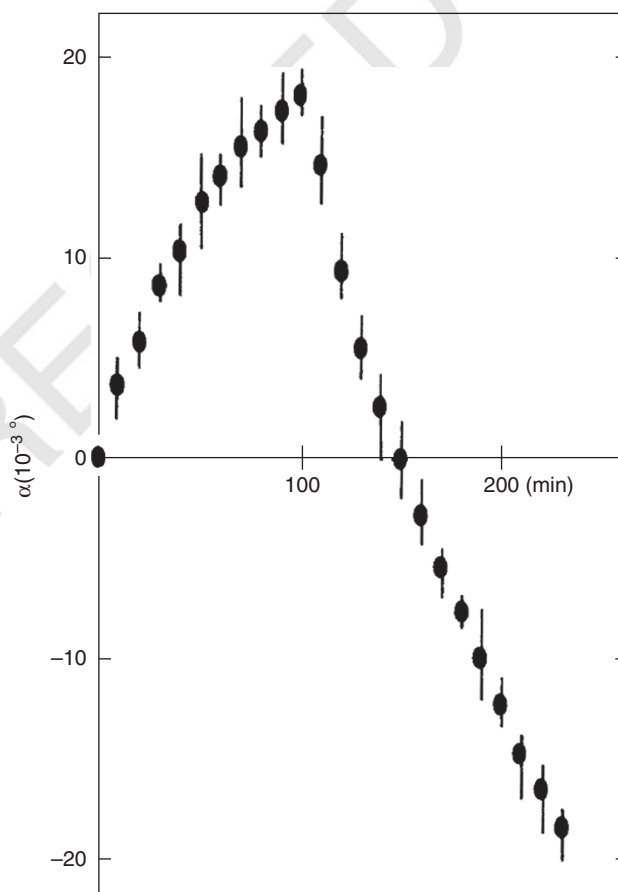


**Figure 7.1.** The time-dependence of the photoinversion of  $\text{Cr}(\text{acac})_3$  [23]. (Reproduced by permission of the Chemical Society of Japan.)

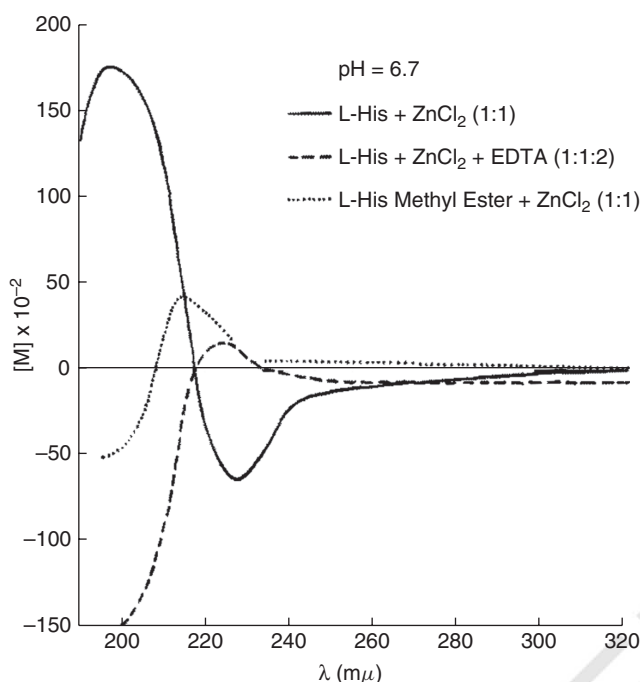


**Figure 7.2.** Chelation of Zn(II) by histidine studied by ORD [24]. (Reproduced by permission of the American Chemical Society.)

### 7.2.3. Conformational Studies by Optical Rotatory Dispersion: L-Histidine Chelation

In the context of studies probing the effect of metal ions in biological systems, ORD was used to show that metal ions induce a change in conformation of L-histidine upon chelation [24]. L-Histidine itself exhibits a positive Cotton effect in the absence of metal ions. Upon chelation with transition metals such as Zn(II) (Figure 7.2) Co(II), Ni(II), and Cu(II), a negative Cotton effect of greater amplitude appeared. Addition of two equivalents of ethylenediaminetetraacetate (EDTA) restored the optical rotatory dispersion (ORD) curve of free L-histidine. Chelation with metal ions resulted in a change in conformation that was highly improbable for the free L-histidine in solution. These observations are consistent with the well-known sensitivity of ORD to conformation, which is highly responsive to metal chelation.

### 7.2.4. Metal-Binding Induced Dynamic Stereochemistry in a Biopolymer Monitored by Optical Rotation and Optical Rotatory Dispersion

In another study of the effect of metals on biological molecules, ORD spectroscopy was used in various studies of the conformational behavior of biopolymers. The tryptic peptide comprising residues 38–61 of oxidized bovine pancreatic ribonuclease A was isolated and shown to be convertible to a helical conformation in 2-chloroethanol- or 2,2,2-trifluoroethanol–water mixtures [25]. The characteristic trough in the optical rotatory dispersion spectrum near 233 nm associated with the helical conformation was progressively reduced by addition of each of 3 eq of  $\text{Cu}^{2+}$  (Figure 7.3). The depth of the trough was regained quantitatively by addition of an equivalent amount of EDTA. The

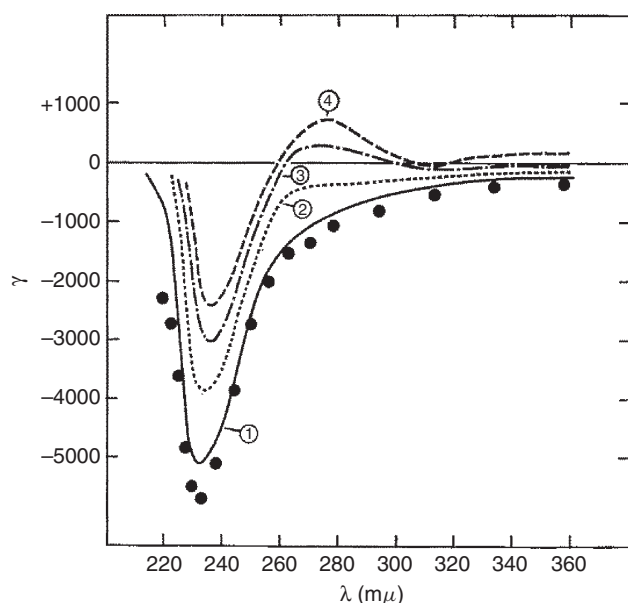


**Figure 7.3.** Effect of stepwise addition of  $\text{Cu}^{2+}$  on ORD curves for peptide dissolved in 50% aqueous 2,2,2-trifluoroethanol. Curve 1, curve for the peptide at an apparent pH of 10.0; curves 2, 3, and 4, results after addition of 1, 2, and 3 equivalents of  $\text{Cu}^{2+}$ . •, values obtained after addition of 3 moles of EDTA [25]. (Reproduced by permission of the American Society for Chemistry and Molecular Biology.)

absorption and optical rotatory spectra of the cupric peptide complexes were qualitatively similar to those of some smaller peptides in which chelation by amide nitrogen atoms of peptide bonds has been demonstrated. The effect of  $\text{Cu}^{2+}$  binding on the helix content was due to the conformational incompatibility of the chelate complexes with the  $\alpha$ -helix.

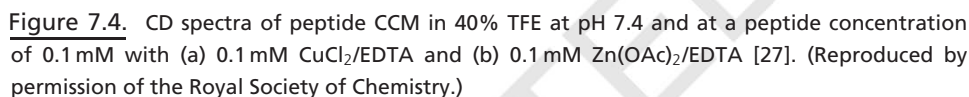
### 7.3. METAL-BASED SWITCHES MONITORED BY ELECTRONIC CIRCULAR DICHROISM (ECD)

ECD has been the dominant chiroptical technique used to probe metal-based switches in recent times. With the availability of many examples, this section will be organized by the triggering method, and the role of ECD in characterizing the dynamic stereochemical phenomena will then be discussed in context.

#### 7.3.1. Metal-Binding Induced Dynamic Stereochemistry

**7.3.1.1. Metal-Binding-Induced Dynamic Stereochemistry in Biological Polymers.** In a more recent study of metal ions interacting with biological polymers, the Woolfson group designed and characterized a peptide that reversibly switches between a trimeric  $\alpha$ -helical coiled coil and a zinc-bound folded monomer [26]. Kokschi and co-workers [27] constructed a simple system to study of the impact of different metal ions on peptide secondary structures. The design was based on an  $\alpha$ -helical coiled coil peptide. Histidine mutations were incorporated into the heptad repeat (Figure 7.4) to generate possible complexation sites in the target peptide CCM for  $\text{Cu}^{2+}$  and  $\text{Zn}^{2+}$  ions, which was shown to be a strong trigger for a secondary structure switch from an  $\alpha$ -helix (structure 1) to a  $\beta$ -sheet (structure 2). The capture of  $\text{Cu}^{2+}$  and  $\text{Zn}^{2+}$  ions by EDTA reversed the  $\beta$ -sheet formation to an  $\alpha$ -helical structure, as revealed by CD spectra. Therefore, switching between  $\alpha$ -helix and  $\beta$ -sheet was easily controlled in both directions.





**7.3.1.2. Metal-Binding-Induced Dynamic Stereochemistry in Synthetic Polymers..** Chiroptical response to metal ion binding has also been studied in synthetic polymer systems. Kakuchi and co-workers [28] reported that a poly(phenylacetylene) bearing a polycarbohydrate ionophore as a graft chain, copolymer **3**, showed a split-type circular dichroism (CD) in the long absorption region of the conjugated polymer backbone (280–500 nm) which varied in response to different metal ions (Figure 7.5). The CD of **3** strongly depended on the radii of the guest metal cations. A metal cation whose ionic radius was 1.16 Å or greater, such as Ba<sup>2+</sup>, decreased the amplitude and eventually caused an inversion while those with radii smaller than 1.16 Å, such as Co<sup>2+</sup>, only decreased the amplitude without inversion. This suggested that copolymer **3** underwent a helix–helix transition through the host–guest complexation with achiral inorganic metal cations.

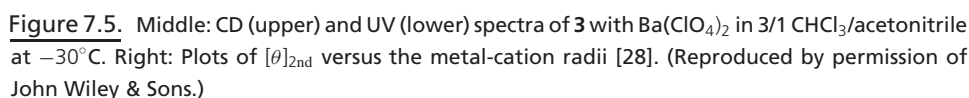


**Figure 7.5.** Middle: CD (upper) and UV (lower) spectra of **3** with Ba(ClO<sub>4</sub>)<sub>2</sub> in 3/1 CHCl<sub>3</sub>/acetonitrile at −30°C. Right: Plots of [ $\theta$ ]<sub>2nd</sub> versus the metal-cation radii [28]. (Reproduced by permission of John Wiley & Sons.)

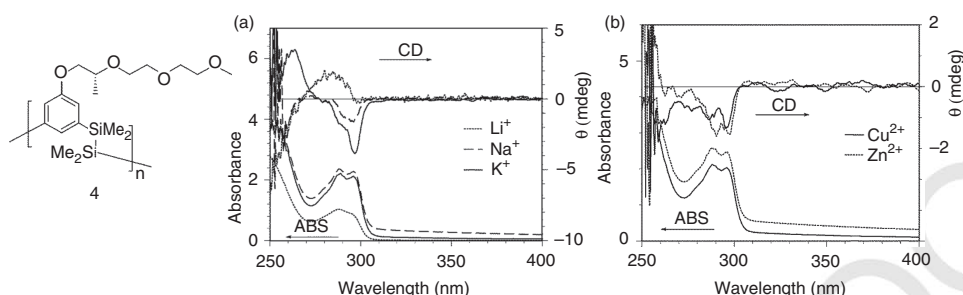


**Figure 7.6.** Absorption and CD spectra of **4** in dichloromethane in the presence of metal ions: (a) Li(OTf) (dotted line), Na(OTf) (dashed line), and K(OTf) (solid line). (b) Cu(OTf)<sub>2</sub> (solid line) and Zn(OTf)<sub>2</sub> (dotted line) [29]. (Reproduced by permission of the American Chemical Society.)

Sanji, Tanaka, and co-workers [29] reported that the  $\sigma_{(\text{Si}-\text{Si})}-\pi$  conjugated poly(*m*-phenylenedisilanylene) with a chiral tri(ethylene glycol) side chain, **4**, displays optical activity arising from metal-coordination interactions (Figure 7.6). Interaction of the side chains with the metal ions is sensitive to the size and the coordination mode of the metal ions, selectively inducing twist sense bias of the helical conformation to display optical activity. Li<sup>+</sup> induced a positive CE, while complexation with Na<sup>+</sup> or K<sup>+</sup> gave a negative CE. Very little CE was observed upon addition of Mg<sup>2+</sup> or Ca<sup>2+</sup> and a negative CE appeared when complexed with Cu<sup>2+</sup> or Zn<sup>2+</sup>. The metal-induced chirality in polymer **4** is reversible: No CD signals were observed when the solution was washed with water to remove the metal ions.

**7.3.1.3. Electron-Switched Supramolecular Chiral Polythiophene Aggregates.** In a system showing supramolecular complexity, Goto and Yashima [30] reported electron-switched supramolecular chiral polythiophene aggregates. Polythiophene oligomers with side chains containing remote chiral centers form chiral aggregates in certain solvents that exhibit induced circular dichroism (ICD) in the  $\pi-\pi^*$  transition region. Addition of a Cu(II) salt resulted in oxidative doping of the polymer main chain and the disappearance of CD. Further addition of amines such as triethylenetetramine removed the doping by shifting the oxidation potential of the copper, extracting electrons from the polythiophene molecules and consequently regenerating the ICD signal. Doping also induced color and morphological changes as measured by electronic absorbance and atomic force microscopy. Besides using chirality to probe fundamental interstrand interaction phenomena [31], chiral oligothiophenes have been examined for applications involving circular polarized electroluminescence [32] as well as enantioselective sensors, electrodes, catalysts, and adsorbents [33, 34]. Electron-induced triggering of polythiophenes would bring new dimensions to such devices if adaptable in the solid state.

### 7.3.2. Environment-Induced Switches

Chiroptical properties of metal complexes respond to a startling variety of environmental triggers including counterion, temperature, solvent, and pressure. In 1931, Pfeiffer and Quehl [35] reported that the optical rotation of a solution of an optically active compound (the “environment” compound) changes upon the addition of racemic mixtures of some



optically active coordination compounds, which is generally referred to as the “Pfeiffer effect.” This effect has been attributed to the observed shift of enantiomeric equilibrium due to an outer-sphere association of the racemic metal complex and the chiral additive. The perturbation of the equilibrium leads to an unequal diastereomer occupation [36]. We will not discuss this effect in detail here, but we will cite several recent environment-induced stereodynamic systems that are conceptually related to the Pfeiffer effect.

**7.3.2.1. Guest-Controlled Tripodal Ligand Chirality.** Supramolecular conformational bias based on host–guest complexes includes nonempirical CD approaches for the determination of the absolute configuration of primary amines [37]. Complexation of the conformational racemate  $[\text{Cu}(\text{BQPA})](\text{ClO}_4)_2$  ( $\text{BQPA} = N, N$ -bis[2-quinolyl]methyl- $N$ -[2-pyridyl]methylamine) [38] with various chiral amines gave ECCD spectra that were consistent with formation of a preferred conformational diastereomer. The zinc(II) complexes with solvent coordinated as the fifth ligand exhibit conformational enantiomerism, with the chirality of the molecule originating from the helical structure of the ligand when associated with the metal ion. Introduction of a chiral guest molecule may displace the solvent and create diastereomers. It was observed that left-handed guests induced a left-handed propeller conformation in the ligand, yielding a positive couplet in the CD spectra [39]. The details of the CD spectral assignment were elucidated with chiral ligands and are discussed later in this chapter.

**7.3.2.2. Zinc Porphyrin Tweezers.** Much more sensitive chirality “sensing” was achieved by forming supramolecular complexes of primary chiral amines with pentanediol-linked zinc porphyrins, referred to as a “zinc porphyrin tweezer” [16, 40, 41], as shown in Figure 7.7. Binding occurs first between the chiral primary amine and carrier molecules, which, in turn, bind to the bidentate zinc porphyrin. The resulting 1:1 host–guest complex generates an ECCD spectrum. Based on the sign of the couplet in the split CD spectrum, the group order (small, medium, large) in the Newman projection is determined and the absolute configuration at the chiral carbon of the monoamine can be resolved. This approach offers a sensitive, widely applicable nonempirical advancement for probing chirality of organic compounds. A variety of substrates including aromatic amines, cyclic and acyclic amines, amino esters, amides, and cyclic amino alcohols have been examined by this and similar approaches, and the method has been generalized to substrates with various potential points of ligation, including monodentate compounds [42].

A porphyrin dimer with a shorter ethane bridge linker was reported to display pronounced CD spectra in the presence of monofunctional amines [43, 44]. Supramolecular chirality induction occurs when amines bind to the “face-to-face” *syn* conformation of the achiral bis(zinc porphyrin) resulting in the extended *anti* conformer with an increased helical dislocation. These two forms are easily distinguished spectroscopically. Left- and right-handed screw twists of the bis(zinc porphyrin)-amine diastereomers are due to the absolute configuration of the amines. Several amines with the (*R*) absolute configuration induced ECCD spectra with negative couplets, and amines with (*S*) absolute configuration induced the opposite handedness. It should be noted, though, that this relationship does not necessarily follow since *R, S* configurational assignment follows the CIP-Rule where the atomic number of the substituent attached to the stereogenic center determines *R* or *S* assignment. However, it is steric factors that determine the interporphyrin helicity. The bulkier amines resulted in stronger CD signals, confirming the role of steric factors in the mechanism of chiral induction.

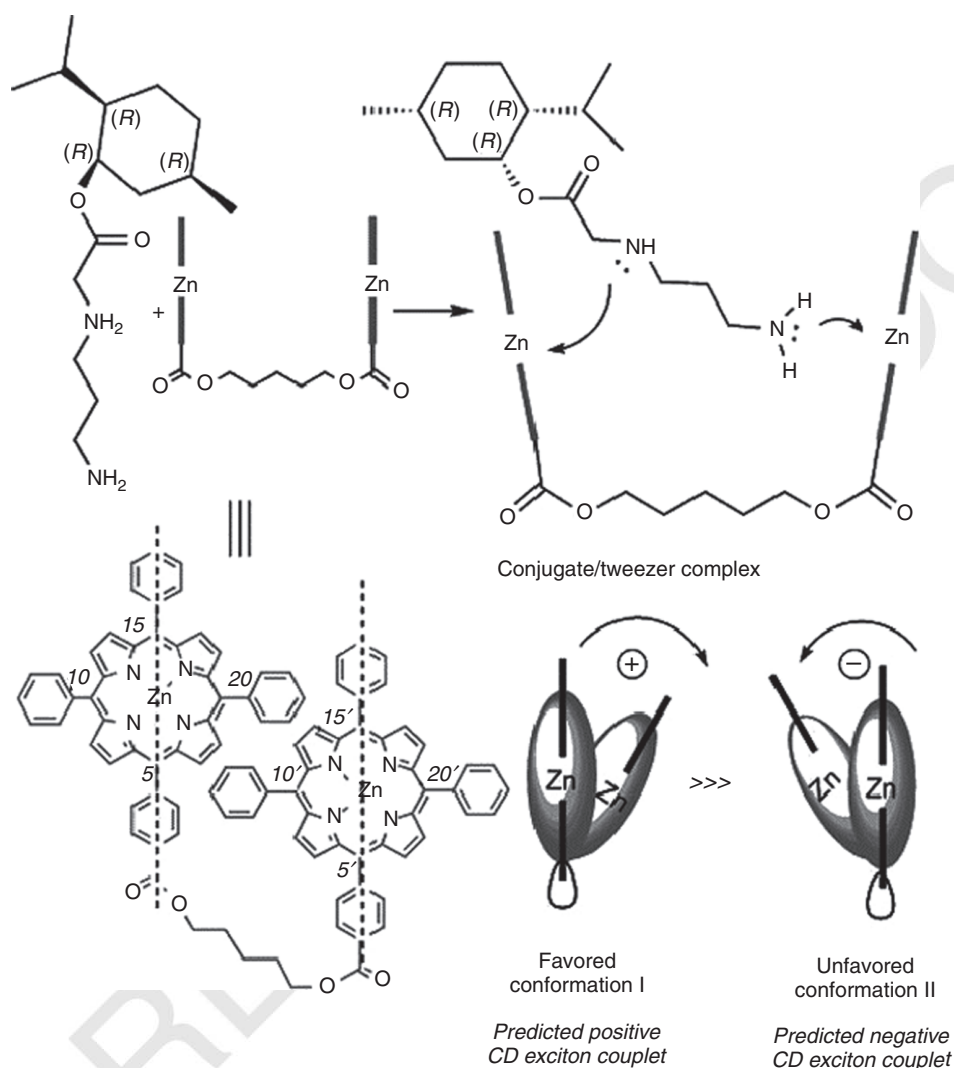


**Figure 7.7.** Macrocyclic 1:1 host-guest complex formed between guest and host. (Reproduced by permission of The Royal Society of Chemistry [16, 41].)

**7.3.2.3. Practical Application of the Pfeiffer Effect for Analyzing Chiral Diamines.** Recently, Anslyn took advantage of Pfeiffer-related phenomena to develop a rapid assay of enantiomeric excess. Chiral diamines were added to racemic Cu(I) or Pd(II) complexes, resulting in CD spectra corresponding to metal-to-ligand charged transfer (MLCT) bands of the metal complexes [45, 46]. An instrument interfaced to a robotic 96-well plate allowed rapid and convenient measurement of the CD spectra of the compound library. Linear discriminate analysis of the CD spectra then determined the identification, concentration, and enantiomeric excess of the diamines. This study represents a practical application of a chiroptical sensor technique.

**7.3.2.4. Anion-Controlled Switching of Amide Complexes.** There are several interesting examples of chiroptical metalloswitches triggered by interaction with

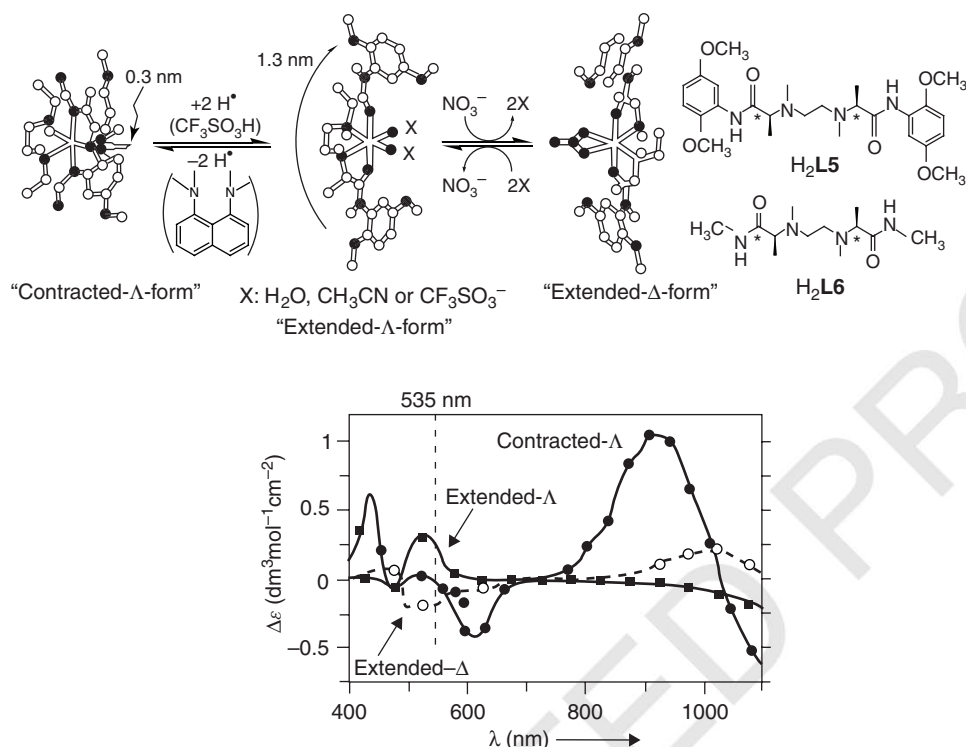


**Figure 7.8.** Stretching and inverting dual motions of the  $\text{Co}^{\text{II}}$  complex. Crystal structures CD spectra of  $[\text{Co}(\text{L5})]$  (left,  $\bullet$  for CD) and  $[\text{Co}(\text{H}_2\text{L5})(\text{CF}_3\text{SO}_3)(\text{H}_2\text{O})](\text{CF}_3\text{SO}_3)(\text{CHCl}_3)$  (middle,  $\blacksquare$ ), as well as DFT-optimized structure of  $[\text{Co}(\text{H}_2\text{L5})(\text{NO}_3)]^+$  (right,  $\circ$ ), are illustrated [50]. (Copyright Wiley-VCH Verlag GmbH & Co. KGaA. Reproduced with permission.)

anions. Interest in such systems is heightened because supramolecular recognition of anions developed later than that of cations, and the abundance of potential anionic analytes in biology and other areas. Yano et al. [47] reported chiral inversion induced around a seven-coordinated cobalt center by interaction between sugars and sulfate anions. New cage-type cobalt(II) complexes that consist of *N*-glycosides from mannose-type aldoses and tris(2-aminoethyl)amine (tren),  $[\text{Co}(\text{aldose})_3\text{tren}]\text{X}_2 \cdot n\text{H}_2\text{O}$  ( $\text{X} = \text{Cl}^-, \text{Br}^-$ ), and  $[\text{Co}(\text{aldose})_3\text{tren}]\text{SO}_4 \cdot n\text{H}_2\text{O}$  exhibited  $\text{C}_3$  helical configuration inversion around the  $\text{Co}(\text{II})$  center. The CD spectral characteristics of  $[\text{Co}(\text{aldose})_3\text{tren}]\text{X}_2 \cdot n\text{H}_2\text{O}$  changed dramatically with the addition of sulfate anions, and even inverted at high sulfate concentrations, suggesting ion pair formation which was confirmed by a crystal structure. When sulfate ion is embedded into the cavity of the sugar hydroxyl groups, the complex adopts a  $\Delta$  configuration, while the complex with the halogen anion exhibits a  $\Lambda$  configuration. When the sulfate anion approaches the sugar complex, the electrostatic attraction between the doubly negative and positive charges of the sulfate anion and complex cation causes the hydrogen bonds between the ligands to be interrupted and brings about a chiral inversion due to the sulfate embedding into the large complex cavity. Reversibility was exhibited when the sulfate ions were removed and replaced with halide ions.

Miyake et al. [48] established that the helicity of a chiral tetradentate ligand (ligand **L6** in Figure 7.8) chelated to  $\text{Co}(\text{II})$  was readily inverted by the addition of nitrate anion. Preliminary studies suggest that two molecules of nitrate serve to invert the helicity

of the ligand. Chelation of the first equivalent to the Co(II) center displaces the two tertiary nitrogens of the bound ligand, while the second equivalent of nitrate disrupts hydrogen bonding of the amide to solvent [49]. Circular dichroism studies indicated that the initial Co(II) complex exhibited a positive CD signal in the range of the  $d-d$  transition (around 530 nm). Upon gradual addition of  $\text{Bu}_4\text{NNO}_3$  the  $d-d$  transition the CD response changes from positive to negative.

These early findings by Miyake led to the synthesis of a chemical device designed to exhibit dual mode motions [50]. This time, a modified version of chiral tetradentate ligand (ligand **L5** in Figure 7.8) including 2,5-dimethoxybenzene moieties attached through amide linkages to the terminals of the ligand was employed. An acid–base reaction of the corresponding cobalt complex triggers an interconversion of coordinating atoms between amide nitrogen atoms and amide oxygen atoms, which causes a stretching (extension/contraction) molecular mode. Inversion of helicity (again from  $\Lambda$  to  $\Delta$ ) after addition of five equivalents of  $\text{Bu}_4\text{NNO}_3$  accounts for the second device mode. CD studies of the  $[\text{Co}(\text{L5})]$  complex in  $\text{CH}_3\text{CN}/\text{CHCl}_3 = 1/9$  exhibit positive signals at 433 nm and 918 nm and negative signals at 474 nm, 607 nm, and 1100 nm, which correspond to the contracted  $\Lambda$ -form. Two equivalents of  $\text{CF}_3\text{SO}_3\text{H}$  (to form  $[\text{Co}(\text{H}_2\text{L5})(\text{CF}_3\text{SO}_3)(\text{H}_2\text{O})](\text{CF}_3\text{SO}_3) \cdot (\text{CHCl}_3)$ ) then caused a rapid signal shift from 0 to positive in the 530-nm region ( $\sim 5$  s) which indicated a switch to the extended  $\Lambda$ -form. The helicity inversion caused by addition of five equivalents of  $\text{Bu}_4\text{NNO}_3$  gave rise to a negative CD signal around 530 nm. The similarity of this CD signal shift to the original  $\text{H}_2\text{L6}$  ligand study supports the assertion that helicity is changed in the device. CD signals remained consistent after many deprotonation/protonation cycles, proving that robust reversibility was established. Such a kinetically labile Co(II) complex provides for a dynamic dual mode switch that could potentially be required for sophisticated supramolecular switching devices.

Recently, pentapeptide chains were combined in such a chirality-switchable Co(II) complex. The peptide chains experienced helix inversion following the helicity inversion of the octahedral metal center upon addition of the  $\text{NO}_3^-$  anion stimulus (Figure 7.9) [51]. Similar peptide helix inversion by nitrate anion was shown to occur in analogous  $\text{Ni}^{\text{II}}$  and  $\text{Zn}^{\text{II}}$  complexes. Selection between  $\text{Zn}^{\text{II}}$ ,  $\text{Co}^{\text{II}}$ , or  $\text{Ni}^{\text{II}}$  allowed tuning of the rate of the inversion process to occur on a timescale from milliseconds ( $\text{Zn}^{\text{II}}$ ) to hours ( $\text{Ni}^{\text{II}}$ ). The estimated half-lifetime ( $\log \tau_{1/2}$ ) of these metallo-peptide complexes showed a linear correlation with the water exchange lifetime of the aqueous metal cations.

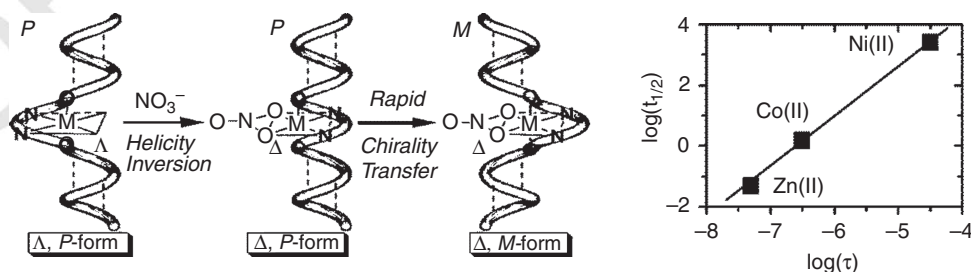


**Figure 7.9.** (Left) Helicity inversion around a metal center and sequential chirality transfer to the pentapeptide helical tubes ( $-\text{Aib}-\Delta\text{Phe}-\text{Aib}-\Delta\text{Phe}-\text{Aib}-\text{OCH}_3$ ). (Right) Linear relationship between half-lifetime ( $t_{1/2}$ ) of helicity inversion and cation water exchange lifetime ( $\tau/\text{s}$ ) [51]. (Reproduced by permission of the American Chemical Society.)

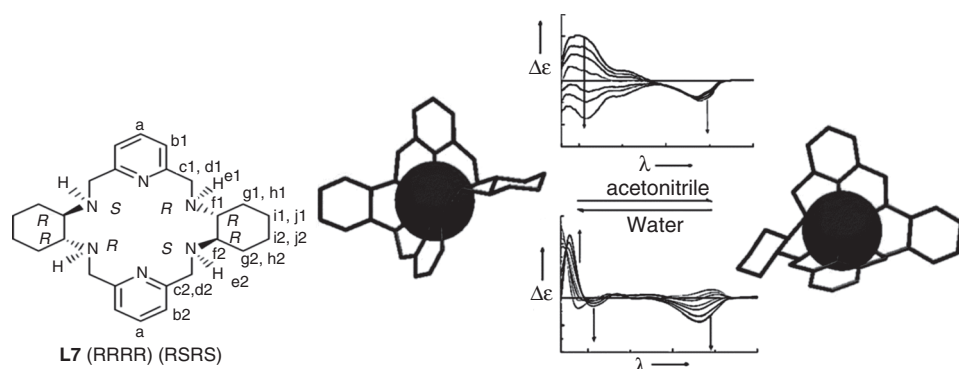


**Figure 7.10.** (Left) Structures of one of the chiral macrocycle isomer  $L7_{(RRRR)(RSRS)}$ . (Right) Solvent induced reversible helicity inversion with accompanying CD spectra [54]. The top spectra show the change in ellipticity over time for the compound on the left upon dissolution in acetonitrile; the bottom spectra are for the compound on the right in water. (Copyright American Chemical Society. Reproduced with permission.)

**7.3.2.5. Solvent-Controlled Switching of Metal Complexes.** Solvent can also induce significant changes in chiroptical response in metal-based systems, either as a result of general differences in polarity or nonspecific solvation or as a result of coordination of solvent in the inner coordination sphere of a metal complex. In a novel study, the Lisowski group has examined chiroptical switches involving lanthanide complexes of chiral hexaazamacrocycles [52, 53]. The hexaazamacrocyclic  $L7$  [54] shown in Figure 7.10 was designed to complex large lanthanides such as Yb(III) and Eu(III). Upon addition of  $Yb(NO_3)_3 \cdot 5H_2O$  in acetonitrile, it was observed that the chiral ligand  $L7$  wrapped around the Yb in a helical  $\Lambda$ -form corresponding to the  $(R, R, R, R)-(S, R, S, R)$   $L7$  isomer. Crystal structure studies of  $[YbL7(NO_3)_2]_2-[Yb(NO_3)_5](NO_3)_4 \cdot 5CH_3CN$  show an improper torsion angle C2–C4–C15–C17 of  $-13.3^\circ$ , which is unusually high for a lanthanide(III) hexaazamacrocyclic complex. Solvation of the same complex in water, though, leads to ligand reorganization presenting a sharp shift in helicity as evidenced by an improper torsion angle C2–C4–C15–C17 of  $87.2^\circ$  for the  $(R, R, R, R)-(S, S, S, S)$  isomer. CD studies confirm helicity inversion by solvent effects, demonstrating quantitative conversion in 144 hours. The proposed mechanism of inversion involves an initial exchange of hydrate into a 10-coordinate metal inner sphere, which is followed by slow ligand reorganization into an 8-coordinate sphere. Lisowski argues that the “squeezed”  $(R, R, R, R)-(S, S, S, S)$  isomer is more capable of accommodating smaller water axial ligands whereas the “open”  $(R, R, R, R)-(S, R, S, R)$  isomer preferentially binds the bulkier nitrate ligand in the axial position [54]. The study as a whole represents a rare case of reversible solvent induced helicity inversion for a metal-based complex.

Recently, Muller, Lisowski, and co-workers [55] reported that a similar but larger chiral nonaazamacrocyclic amine wraps around the lanthanide(III) ions to form enantiopure helical complexes. The NMR and CD spectra show that kinetic complexation product of the  $(R, R, R, R, R, R)$  isomer prefers the  $(M)$ -helicity. However, the preferred helicity of the thermodynamic product is  $M$  for the early lanthanide(III) ions and  $P$  for the late lanthanide(III) ions. In solution, the late lanthanide(III) complexes slowly invert their helicity from the kinetically preferred  $M$  to the thermodynamically preferred  $P$ .

The Mamula group reported the diastereoselective self-assembly of the enantiomerically pure pinene-bipyridine-based receptor,  $(-)$  or  $(+)$   $L$ -, in the presence of Ln(III) ions



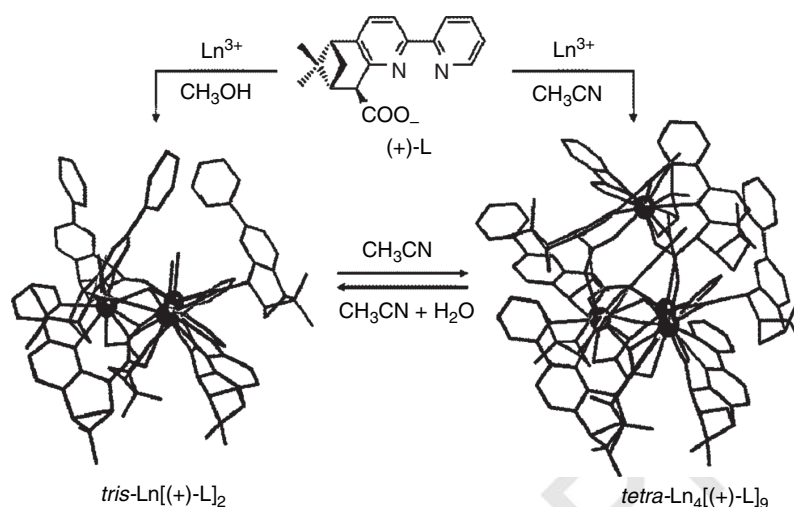


**Figure 7.11.** Divergent self assembly leading to the synthesis of interconverting trinuclear  $[\text{Ln}_3\{(+)\text{-L}\}_6(\mu\text{-OH})]^{2+}$  and tetranuclear  $[\text{Ln}_4\{(+)\text{-L}\}_9(\mu\text{-OH})]^{2+}$  complexes [56]. (Reproduced by permission of the American Chemical Society.)

(Figure 7.11) [56]. Upon exposure to La, Pr, Nd, Sm, Eu, Gd, and Tb ions in dry acetonitrile, it forms a  $C_3$ -symmetrical, pyramidal tetranuclear species with the general formula  $[\text{Ln}_4(\text{L})_9(\mu\text{-OH})(\text{ClO}_4)_2]$  (abbreviated as  $\text{tetra-Ln}_4\text{L}_9$ ). Three metal centers shape the base: an equilateral triangle surrounded by two sets of helically wrapping ligands with opposite configurations. The tetranuclear structure is completed by a capping, helical unit  $\text{LnL}_3$  whose chirality is also predetermined by the chirality of the ligand. The sign and the intensity of the CD bands in the region of the  $\pi-\pi^*$  transitions of the bipyridine are highly influenced by the helicity of the capping fragment  $\text{LnL}_3$ . In methanol, it self-assembles to give the trinuclear species  $[\text{Ln}_3(\text{L})_6(\mu\text{-OH})(\text{H}_2\text{O})_3](\text{ClO}_4)_2$  (abbreviated as  $\text{tris-LnL}_2$ ). The two related superstructures can be interconverted. As is shown by the CD evolution in Figure 7.12, in pure dry acetonitrile, pure  $\text{tris-LnL}_2$  disassembles and reorganizes gradually to form  $\text{tetra-Ln}_4\text{L}_9$ . If a certain amount of water is added,  $\text{tris-LnL}_2$  can be reassembled quantitatively. Water stabilizes the trinuclear species to the detriment of the tetranuclear ones. Reducing the amount of water by molecular sieves leads to the tetranuclear species. However, the number of these reversible cycles is limited due to partial decarboxylation of the ligand in the presence of water.

Recent reports from Nitschke describe a Cu(I) based solvent-triggered molecular switch [57]. The initial synthesis of the chiral Cu(I) complex in methanol resulted in an equal mixture of both *P*- and *M*-diastereomers which was characterized by a weak circular dichroism spectrum bearing similarities to that of the free ligand. A featureless CD spectrum in MLCT band further established that there was no net diastereomeric excess formed. A stark contrast was then encountered when the Cu(I) complex was dissolved in dichloromethane- $d_2$  and the CD spectrum revealed a positive CE in the MLCT region. Combined studies of CD and NMR suggest that the Cu(I) complex (Figure 7.13) fully converts to the *P*-diastereomer in nonpolar dichloromethane. Similar studies in DMSO then showed that the *M*-diastereomer of the complex (Figure 7.13) exists in 20% excess, setting the stage for a reversible metal-based chiroptical molecular switch. The solvent-induced conformational exchange was reasoned to be dominated by hydrogen bonding effects. A weakly polar solvent such as dichloromethane only weakly interacts



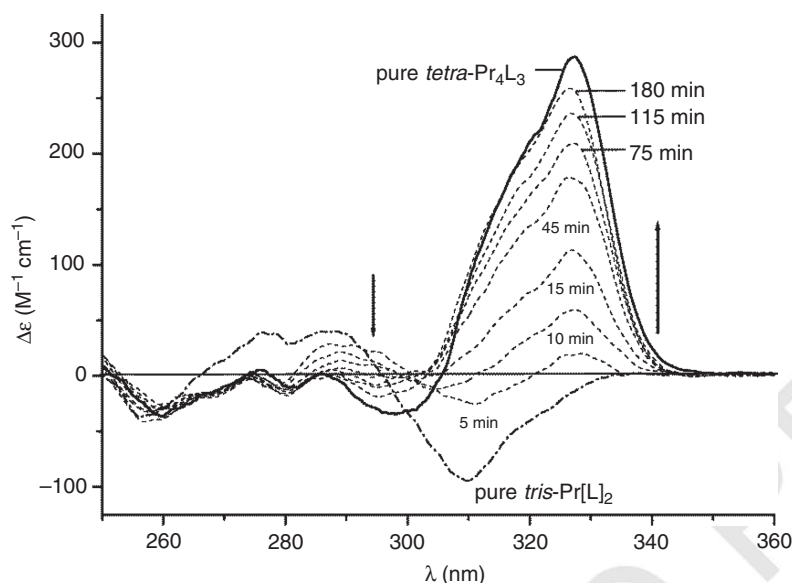


Figure 7.12. Time-dependent evolution of the CD profile of tris-Pr[(+)-L]<sub>2</sub> in CH<sub>3</sub>CN [56]. (Reproduced by permission of the American Chemical Society.)

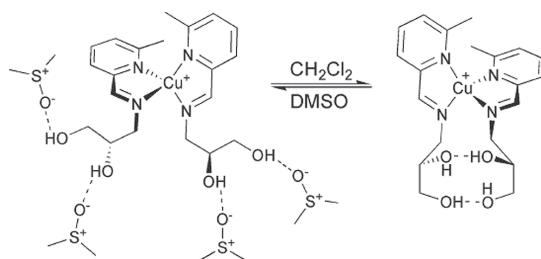


Figure 7.13. Postulated structures in DMSO (left, *M* predominating) and CH<sub>2</sub>Cl<sub>2</sub> (right, *P* exclusively) [57]. (Reproduced by permission of the Royal Society of Chemistry.)

with the hydroxyl groups of the ligand, allowing for intramolecular hydrogen bonding. Such hydrogen bonding serves to rigidify the structure and lock the complex into the *P* conformation. Polar solvents such as DMSO, though, interact strongly with the ligand hydroxyl group and push the hydroxyl groups apart, leading to a preference for the *M* conformation. The authors hypothesize that such a reversible solvent-triggered complex could serve as a means to control stereoselectivity in future metal-catalyzed reactions.

### 7.3.3. Redox-Triggered Systems

The rich coordination chemistry literature offers many avenues for entry into the design of redox-sensitive metal complexes that display rich chiroptical spectra. Redox-active metal ions themselves often show useful electronic spectral changes. However, changes in CD spectra of the organic ligand are also very useful, particularly in complexes that display CD exciton chirality.

**7.3.3.1. Iron Translocation in Triple-Stranded Helical Complexes.** Shanzer and co-workers [58] reported the first published example of a redox-mediated chiroptical redox switch. The system was based on chemical triggering of iron translocation in

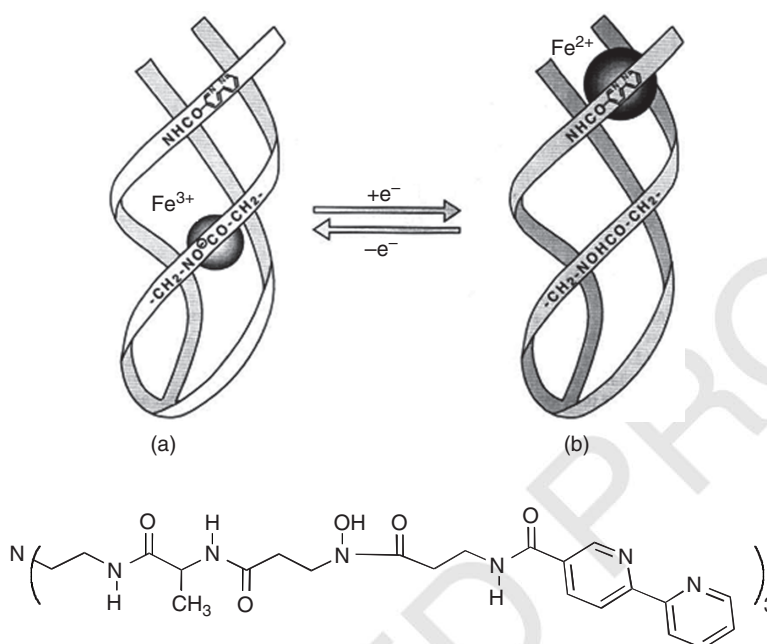


**Figure 7.14.** Tripodal ligand containing two binding sites and the redox-switched chirality of its iron complexes [58]. (Reprinted by permission from Macmillan Publishers Ltd. Copyright 1995.)

triple-stranded helical complexes (Figure 7.14). The design accommodated a single metal ion in one of two sites, either a “hard” binding  $\text{N}_3\text{O}_3$  cavity presenting three hydroxamate moieties or a “soft”  $\text{N}_6$ -cavity with three bipyridyl ligands. Chemical reduction of  $\text{Fe(III)}$  to  $\text{Fe(II)}$  induced the metal to translocate from the hydroxamate binding site to a bipyridyl site, because the “softer”  $\text{Fe(II)}$  favored the site with more nitrogen ligands. Redox switching of the complex was induced by reduction with ascorbate and oxidation with ammonium persulfate.

Pronounced differences in UV-vis and CD spectra were observed corresponding to changes in absorbance associated with  $\text{Fe(II)}$  versus  $\text{Fe(III)}$  electronic spectra. A split CD spectrum in the UV region was observed that was three times more intense for the  $\text{Fe(II)}$  state, suggesting exciton interactions involving the bipyridyl moieties. Reduction was rapid, and oxidation gave the  $\text{Fe(III)}$  absorbance spectrum after a few minutes (several hours were required to achieve the original  $\text{Fe(III)}$  CD spectrum). The fact that metal exchange did not occur between control compounds with single metal binding sites suggested intramolecular translocation reaction. Variation of the structure resulted in significantly different translocation rates.

**7.3.3.2. Chiroptical Tripodal Ligands.** Three-armed, or tripodal, ligand-metal complexes have been found to offer particularly rich stereodynamic behavior, especially when coupled with exciton chirality analysis. The development of redox-triggered chiroptical switches in the Canary laboratory began with the observation that tripodal,  $\text{N}_4$  ligands form stable coordination complexes with divalent metal cations [59, 60]. In the case of  $\text{Zn(II)}$  and  $\text{Cu(II)}$ , the ligand, otherwise conformationally mobile with many conformations, wraps around the metal ion to form a propeller-like complex. In ligands with a single stereogenic center on one of the tripod arms, the helicity of the propeller formed by the

planes of the heterocycles is dictated by this stereocenter. A number of crystallographic structures [61], with few exceptions, established the relationship between the chiral carbon center and the propeller configuration [62]. ECCD established the preponderance of a single propeller conformation in solution, and it tested whether the same configuration was present relative to the carbon center as had been observed in solid-state studies [63]. It was confirmed that Cu(II) and Zn(II) complexes showed ECCD spectra consistent with solid-state propeller-like structures. This method allowed the assignment of the absolute configuration of secondary amines from the sign of the observed excitant couplet. Furthermore, the sign of the couplet discloses the sense of the propeller twist in solution.

The dependence of CD exciton chirality upon the strength of the electronic transition moment, the proximity of the coupled transitions, and the angle between them led to the development of several interesting chiroptical molecular switches. An on/off system was studied involving a tripodal ligand containing three quinoline moieties [64]. The tris(quinoline) compound in Figure 7.15 forms a coordination complex with Cu(II) (**8**) involving the coordination of four nitrogen atoms and affording an exceptionally intense split CD spectrum that results from the additive effect of three ECCD couplets in one molecule. Reduction to the Cu(I) complex in the presence of strongly coordinating thiocyanate ion gave dissociation of one quinoline arm. This resulted in a much weaker ECCD spectrum due to two factors: (1) the dissociation of one quinoline reduces the number of ECCD couplets from three to one, and (2) the less sterically crowded environment around the copper ion allows unwinding of the ligand and reduces the magnitude

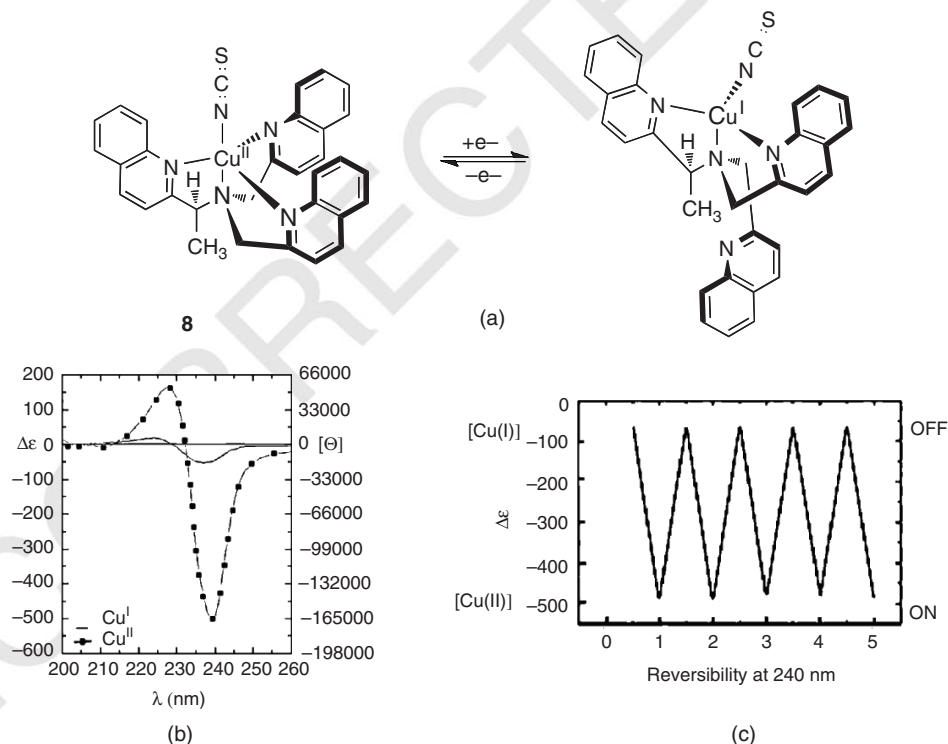


**Figure 7.15.** On/off chiroptical molecular switch. (a) One-electron reduction results in dissociation of an arm of the tripodal ligand. (b) CD spectra of Cu<sup>+</sup> and Cu<sup>2+</sup> complexes. (c) oxidation and reduction cycles with ascorbate and persulfate [64]. (Reproduced by permission of Wiley-VCH.)

of the dihedral angle and therefore diminishes the amplitude of the ECCD couplet. The overall effect is a very large difference in ECCD amplitude between Cu(I) and Cu(II) states. Dependence of the ECCD amplitude on the counterion supported the structural assignment [65]. The complex is highly reversible chemically upon oxidation of the Cu(I) complex with ammonium persulfate and reduction of the Cu(II) complex with sodium ascorbate. Temperature-dependent  $^1\text{H}$  NMR studies of this system led to the conclusion that the two arms lacking the chiral carbon center are in rapid equilibrium between associated and dissociated states at room temperature, but slow on the  $^1\text{H}$  NMR timescale at low temperature [66]. The arm containing the chiral carbon center, however, remains coordinated.

Such tripodal ligands were found to act as chemosensor molecules; their ability to torque a nematic into a cholesteric liquid crystalline phase increased upon complexation with copper ion [67]. Changes in overall shape of the complexes induced by different metals and counterions were transferred sensitively to the supramolecular level, observed by proportionate changes in the degree of twisting. Redox changes (Cu(I)/Cu(II)) also gave large changes in twisting power. The handedness of the induced cholesteric phase was related to the stereochemistry of the ligand. Interestingly, a direct correlation was observed between helical twisting power and ECCD amplitude, consistent with each technique responding proportionately to the relative twist of the planes of the nitrogen heterocycles.

Another related complex containing two chiral carbon centers within a piperidine ring (**9**) was reported (Figure 7.16) [68]. In this case, the rigidity of the ligand provided control as to which chair form of the piperidine was adopted. In the Cu(I) oxidation state, the ligand adopts a relatively stable cyclohexane chair conformation, with two equatorial and one axial substituent. This conformation places one pyridine moiety remote from the metal ion, but this is accommodated by the lower coordination number of the Cu(I) ion. In the Cu(II) state, strong binding to the higher-coordination number ion brings all three pyridines into association, which forces the piperidine to adopt a higher-energy chair with two axial and one equatorial substituents. The CD spectrum of the Cu(II) complex showed the largest amplitude of any complex in this series, but the Cu(I) spectrum did not give an exciton chirality spectrum. In this case, the Cu(I) structure was characterized by a series of  $^1\text{H}$  NMR experiments.

In these studies, CD exciton chirality served as a tool to gauge not only the configuration of the propeller conformation but also the degree of twist of the molecule. Relatively few spectroscopic probes are available to report 3D molecular geometry, so it may be expected that this technique should be broadly applicable for the characterization of solution species [16].

Systematic exploration of amino acid derivatives by Canary and co-workers [69, 70] led to the discovery of a molecule that inverts helicity and CD couplet sign upon one-electron redox change [71]. A ligand derived from the amino acid methionine forms a tetradentate complex with Cu(II) involving three nitrogen atoms and a carboxylate (Figure 7.17). In this system, the propeller twist of the molecule is dictated by the asymmetric carbon center by virtue of a gearing mechanism between the methine and methylene carbon atoms, and it can be visualized when viewing down the bond between the tertiary amine nitrogen atom and the Cu(II) ion. Upon reduction to Cu(I), the ligand reorganizes and the sulfide moiety replaces the carboxylate, which is expected due to the preference of Cu(I) for this type of coordination. The reorganization requires a pivot about the bond between the tertiary nitrogen atom and the asymmetric carbon atom. This pivot destroys the gear previously mentioned; to retain the geared conformation, the

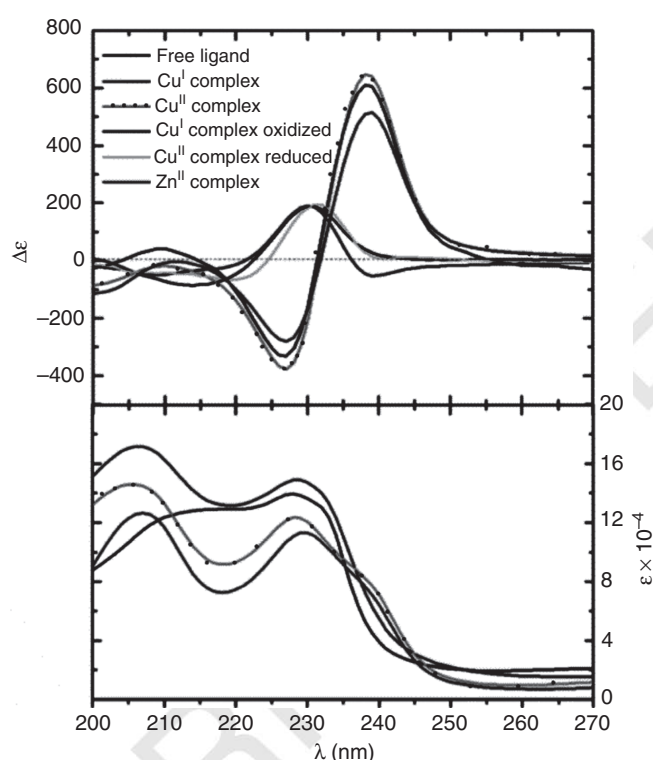
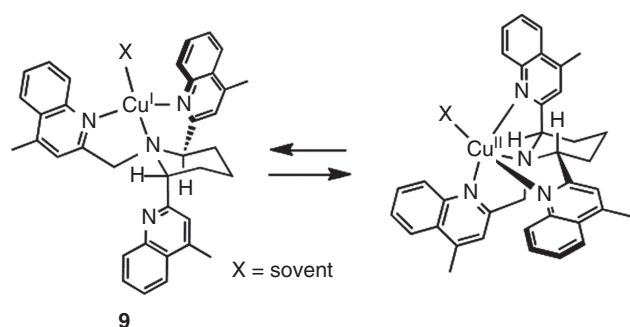


**Figure 7.16.** Redox-triggered inversion of one chair form of a piperidine ring into the other chair and corresponding CD (top) and UV-vis (bottom) spectra [68]. (Reproduced by permission of the American Chemical Society.)

two methylene carbon groups flip, which, in turn, inverts the helical orientation of the two quinoline moieties and, therefore, the exciton chirality spectrum. The CD spectrum appears to give mirror images for the  $\text{Cu}(\text{I})$  versus  $\text{Cu}(\text{II})$  complexes. The switching was reversible with cyclical additions of ascorbate and ammonium persulfate. Crystallographic data supported the structural assignments [72]. The  $\text{Cu}(\text{I})/\text{Cu}(\text{II})$  complexes of other tripodal ligands also give inversion of the CD spectrum including derivatives of methioninol and *S*-methyleysteine [73].

**7.3.3.3. Redox-Controlled Molecular Flipper Based on a Chiral Cu Complex.** Copper redox chemistry has also been explored in other ligand platforms for redox-dependent chiroptical effects. A molecular bipaddled flipper based on a tetradentate chiral Cu complex was reported whose paddling motion could be controlled



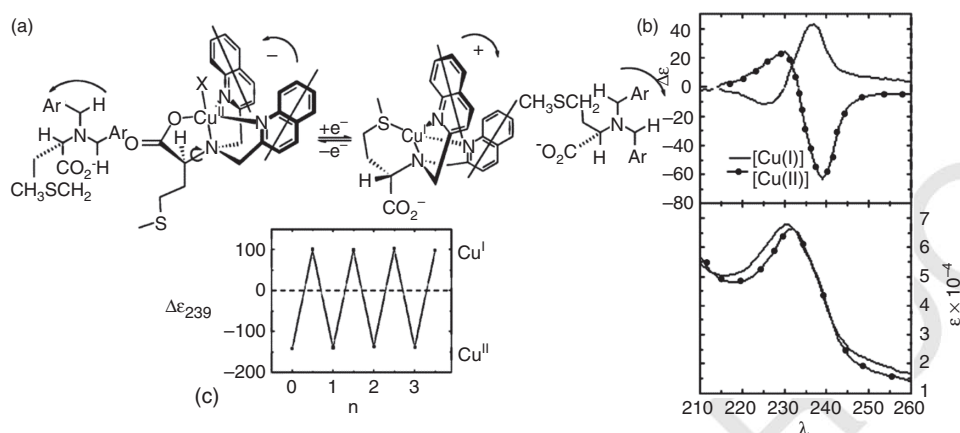


**Figure 7.17.** Redox-induced inversion of helicity. (a) As a result of the presence of gearing among the three arms of the tripod near the sterically crowded tertiary amine of the ligand, a pivot about a C–N bond results in the inversion of the propeller. (b) CD and UV–vis spectra of Cu<sup>+</sup> and Cu<sup>2+</sup> oxidation states. (c) chemical cycling with ascorbate and persulfate [71]. (Reproduced by permission of the American Association for the Advancement of Science.)

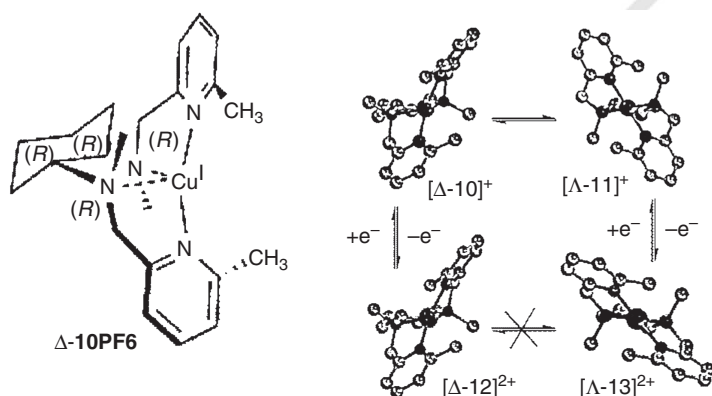


**Figure 7.18.** Crystal structure of  $[\Delta-10]^+$  (top left) and DFT structures of  $[\Lambda-11]^+$  (top right),  $[\Delta-12]^{2+}$  (bottom left), and  $[\Lambda-13]^{2+}$  (bottom right) [74]. (Reproduced by permission of the American Chemical Society.)

by reversible oxidation of the metal center (Figure 7.18) [74]. The isomeric pair of Cu(I) complexes  $\Delta$ -[Cu<sup>I</sup>((N<sub>R</sub>, N<sub>R</sub>, R, R)-L)]PF<sub>6</sub> ( $\Delta$ -10PF<sub>6</sub>) and  $\Lambda$ -[Cu<sup>I</sup>((N<sub>S</sub>, N<sub>S</sub>, R, R)-L)]PF<sub>6</sub> ( $\Lambda$ -11PF<sub>6</sub>) interconvert, a slight preference for  $\Lambda$ -11PF<sub>6</sub>, ( $K_{eq} = 1.3$ ), which can be monitored by time-dependent CD starting with a pure  $\Delta$ -10PF<sub>6</sub> in CH<sub>2</sub>Cl<sub>2</sub> (Figure 7.19a). The amplitude of the Cotton effects decreased with time and eventually rested at smaller amplitudes with opposite signs within a couple of hours. The inversion of the chirality of the aliphatic N atoms resulted in the inversion of helicate chirality.

The mechanical motion undergone by  $\Delta$ -10PF<sub>6</sub> and  $\Lambda$ -11PF<sub>6</sub> could be switched on/off by reversible metal oxidation and reduction electrochemically or chemically. An oxidation experiment of species  $\Delta$ -10PF<sub>6</sub> with AgBF<sub>4</sub> was performed at different times of the isomerization process and the CD of the resulting Cu(II) species ( $\Delta$ -12PF<sub>6</sub> and/or  $\Lambda$ -13PF<sub>6</sub>) recorded (Figure 7.19b). The spectra varied, depending on when the oxidant was added, which corresponded to the degree of  $[\Delta-10]^+ / [\Lambda-11]^+$  isomerization. However, when AgBF<sub>4</sub> was added to a pure  $\Delta$ -10PF<sub>6</sub> sample, all of the  $\Delta$ -10PF<sub>6</sub> was oxidized to  $\Delta$ -12PF<sub>6</sub> and no isomerization to  $\Lambda$ -13PF<sub>6</sub> or  $\Lambda$ -11PF<sub>6</sub> was observed. The transition



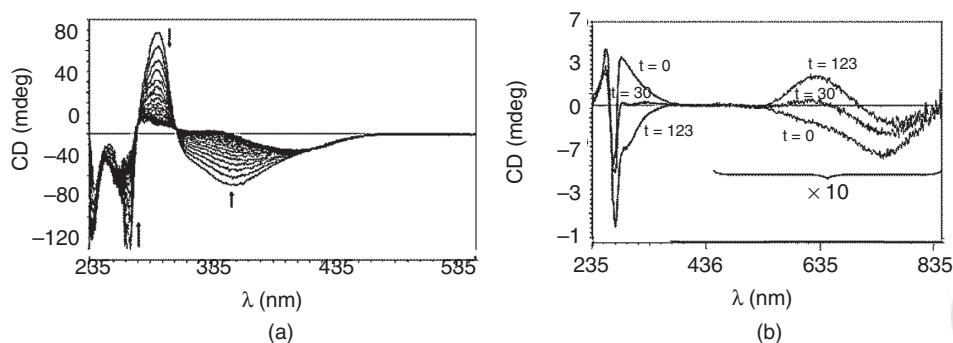


**Figure 7.19.** (a) CD monitoring of the  $\Delta$ -10PF<sub>6</sub>/ $\Lambda$ -11PF<sub>6</sub> isomerization reaction in CH<sub>2</sub>Cl<sub>2</sub>. (b) CD spectra of the oxidized  $\Delta$ -10PF<sub>6</sub>/ $\Lambda$ -11PF<sub>6</sub> couple with AgBF<sub>4</sub> at different isomerization times yielding [ $\Delta$ -12]<sup>2+</sup> at  $t = 0$  min and mixtures of [ $\Delta$ -12]<sup>2+</sup> and [ $\Lambda$ -13]<sup>2+</sup> at  $t > 0$  min [74]. (Reproduced by permission of the American Chemical Society.)

metal integrated into this device acts as a redox switch that permits one to start/stop the motion at will.

**7.3.3.4. Redox-Switchable Pt-Bridged Cofacial Diporphyrins via Carbon–Metal  $\sigma$  Bonds.** In one of several porphyrin-containing systems, Shinokubo, Osuka, and co-workers [75] reported the construction of a Pt(IV)-bridged cofacial diporphyrin architecture and its dynamic helical conformational change by reduction of the bridge to Pt(II) (Figure 7.20). Two stable Pt–C  $\sigma$  bonds supported by the pyridyl groups brought two porphyrin macrocycles to be in close proximity in each of these two complexes. The platinum bridge offers conformational flexibility to the complexes due to the susceptibility of platinum toward redox reaction. These complexes also exhibit helical chirality. Reduction of *M* spiral of **14M** mainly yielded the *P* spiral enantiomer of **15P**. The Pt(IV) complex **14M** exhibits exciton coupling in both UV–vis and CD, while there is no exciton coupling in the Pt(II) complex **15P**.

**7.3.3.5. Redox-Triggered Porphyrin Tweezers.** Recently, a redox-triggered porphyrin tweezer was reported in an attempt to develop materials with optical properties in the visible region of the electromagnetic spectrum [76]. As shown in Figure 7.21, bis(porphyrin) methioninol derivative (**16**) gave a strong ECCD couplet upon metallation with Cu(II). The free ligand and Cu(I) complex did not give ECCD. The absence of an ECCD couplet in the Cu(I) complex was rationalized as resulting from relatively weak association of the metal under the conditions studied. The Cu(II) complex, however, showed very strong amplitude, affording an on/off chiroptical molecular switch. Other, nonchiral electrochemically responsive dimeric porphyrin systems have been reported where the redox changes occurred within the porphyrin moieties [77].

**7.3.3.6. Redox-Controlled Dinuclear Ruthenium-Based Switches Monitored by Electronic Near-IR CD.** A system showing strong changes in near-infrared (NIR) CD spectra was reported recently [78]. NIR techniques are of interest for several reasons, including the benefit of lower incident light energy on organic materials and greater transparency of NIR light in biological applications. Building on earlier studies of organic-based systems [79–81], the Wang laboratory studied dinuclear ruthenium complexes with 1,2-dicarbonylhydrazido bridging ligands  $\Delta$ ,  $\Delta$ -**17** and  $\Lambda$ ,  $\Lambda$ -**17**

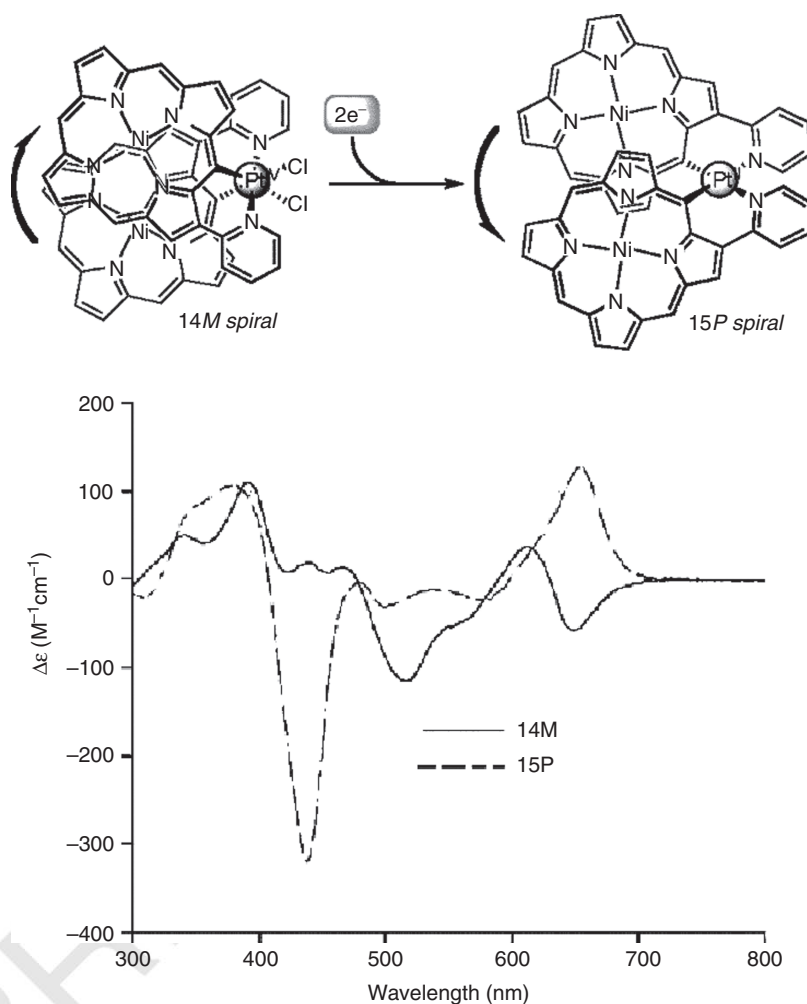


**Figure 7.20.** (Top) Reduction of the *M* spiral Pt(V) complex **14M** result in *P* spiral Pt(II) complex **15P**. (Bottom) CD spectra. [75]. (Reproduced by permission of the American Chemical Society.)

(Figure 7.22) that are highly electrochromic with absorption bands near 500, 900, and 1200–1600 nm. Ligand-centered transitions in the UV region and redox-sensitive MLCT bands in the visible region dominate the CD spectra shown in Figure 7.22. A prominent band near 1115 nm observed in the Ru(II)/Ru(III) state, due to metal–metal charge transfer (MMCT), did not give a strong Cotton effect in the CD spectrum. The Ru(III)/Ru(III) state gave a strong MLCT band at 900 nm that gave a relatively strong Cotton effect in the CD spectrum. Reversible redox switch behavior was demonstrated by monitoring the CD signal at 890 nm and cycling up to seven times electrochemically between the Ru(II)/Ru(II) and Ru(III)/Ru(III) states.

A variety of systems have thus been examined for redox-active metal ion triggered chiroptical molecular switches. The mechanisms reported involve translocation of a metal

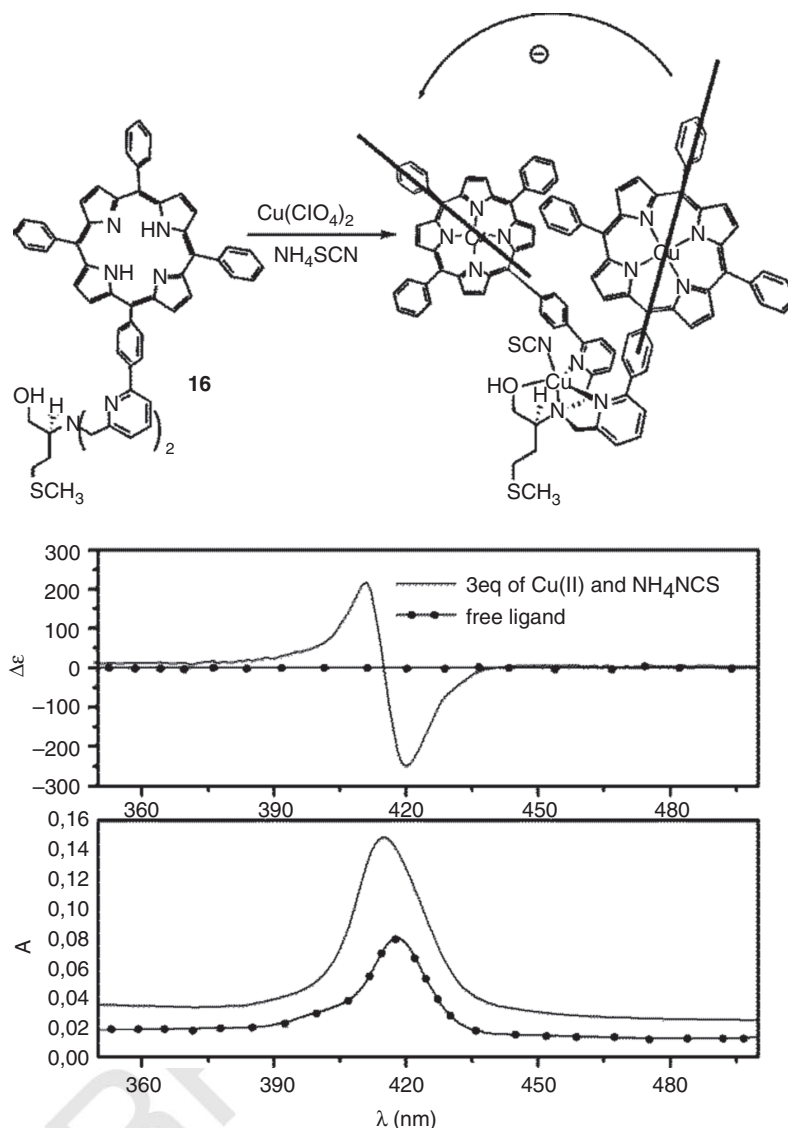
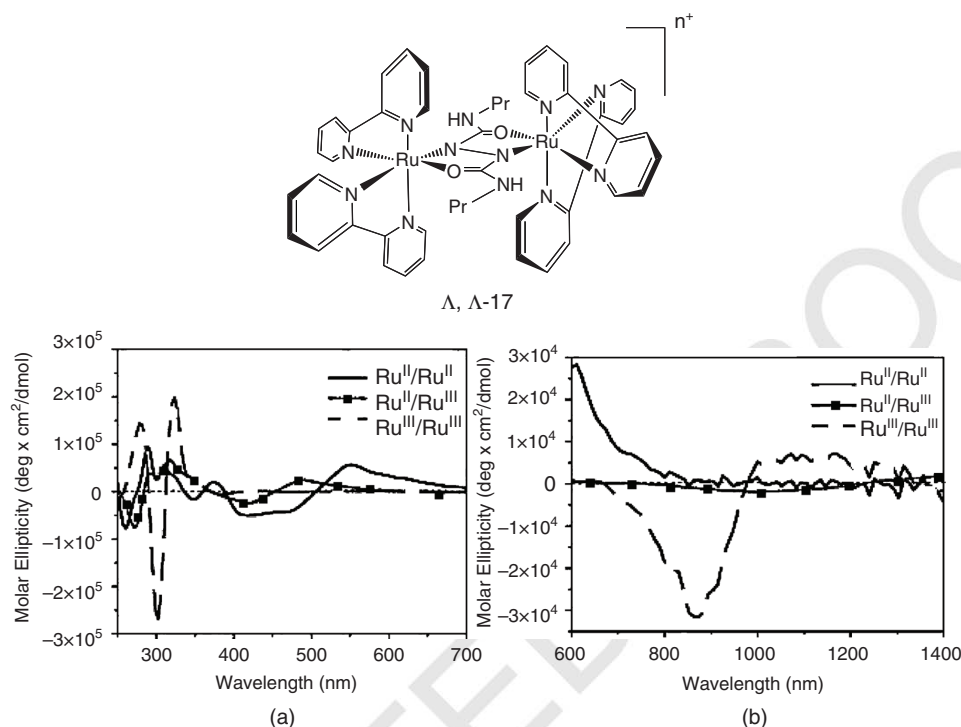


Figure 7.21. Redox-triggered reorientation of porphyrins [76]. (Reproduced by permission of the American Chemical Society.)

ion, changes of lability of ligand rearrangement, or inner sphere ligand rearrangement resulting from change in coordination number or hardness of the metal. The changes in amplitude of observed CD spectra can be dramatic, even leading to complete inversion of the sign of the ECCD couplet.

### 7.3.4. Photochemically Triggered Chiral Metal Switches

Among many interesting studies, the Aida group used ECD to characterize a redox-triggered system in which chemical or photoreduction of a chiral cerium bisporphyrinate double-decker complex resulted in racemization by acceleration of the porphyrin ligand



**Figure 7.22.** CD spectra of  $\Lambda, \Lambda$ -isomer of a diruthenium complex **17** at different oxidation states [78]. (Reproduced by permission of the Royal Society of Chemistry.)

rotation. They further showed that oxidation of a chiral zirconium complex resulted in deceleration of acid-induced racemization [82].

**7.3.4.1. Azobenzene-Based Molecular Scissors.** The Aida group carried out the synthesis of other complex light-triggered chiroptical molecular switches. Life-sized scissors having a handle, pivot, and blades inspired the preliminary design of a pair of molecular “scissors” [83]. The chemical equivalents to these three units were found to be azobenzene as the handle, ferrocene as a pivot, and phenyl groups as the blades (Figures 7.23a and 7.23c). The operation of the molecular scissor is quite elegant. Under standard conditions, the azobenzene handle is predominantly in the *trans* state leading to “closed” blades. Upon irradiation of UV light, the azobenzene undergoes isomerization to the *cis* isomer, which then causes a slight rotation of the cyclopentadienyl rings of the ferrocene pivot. This finally moves the attached phenyl rings away from one another, leading to an “open” scissor state. The scissors’ chirality (due to the planar 1,1',3,3'-tetrasubstituted ferrocene) allows both open and closed states to be seen using circular dichroism (Figure 7.23b). The authors explain that the *trans*-to-*cis* isomerization of [CD(−)280]-*trans*-**18** upon UV-irradiation ( $\lambda = 350$  nm) after 180 s gave rise to CD spectral changes at 240–300 nm due to the major adsorption of the tetraarylferrocene unit. Upon irradiation with visible light ( $\lambda > 400$  nm), a reverse spectral change occurred, where the system quickly reached a photostationary state in 15 s. Effective reversibility was also exhibited by the system upon sequential irradiation with UV and visible light.

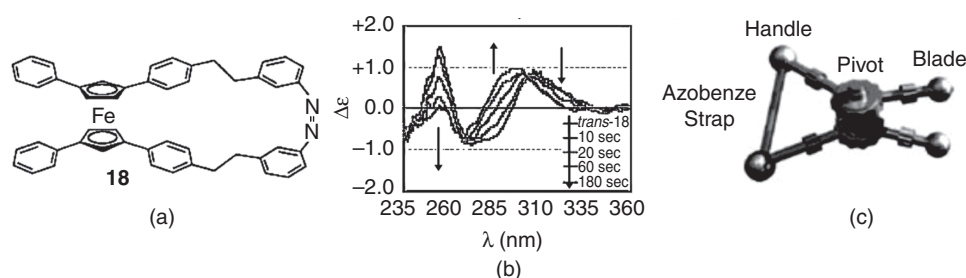


**Figure 7.23.** (a) Structural representation of azobenzene controlled “molecular scissors.” (b) CD spectral changes of *trans*-18 upon irradiation with UV light. (c) Graphic conceptualization of the “molecular scissors” [83, 86]. [Reproduced by permission of the American Chemical Society (a, b) and the Royal Society of Chemistry (c).]

**7.3.4.2. Host-Controlled Guest Chirality.** Further research into Aida’s molecular scissors proved that they could be applied to the field of host–guest chemistry [84]. When metallated porphyrins were attached to the 4-position of the phenyl blades, it was found that a diisoquinoline guest was able to chelate to the zinc porphyrin units. Upon irradiation of the host–guest complex with UV light ( $\lambda = 350 \pm 10$  nm), the *trans*-azobenzene unit again isomerizes to the *cis*-isomer, causing a long-distance conformational twist of the diisoquinoline guest (Figure 7.24). The guest molecule (**19**) in solution is initially achiral due to its conformational freedom; but when added to the host molecule (*trans*-**20**), it binds in a nonplanar CD-active chiral geometry. Overlap of CD bands (275–350 nm) from the host molecule required that differential CD spectra be used to examine the motion of the guest (Figure 7.24b). Irradiation with UV light caused the Cotton effects at 270–350 nm of the guest (**19**) to diminish and then vanish. It is reasoned that the disappearance of the CD band is caused by the guest molecule being forced into a nearly planar state when bound to the *cis*-isomer of the host compound. Sequential irradiation of host–guest complex (**19** • *trans*-**20**) with UV and visible light proves that the complex is controllably reversible (Figure 7.24c). This represents the first instance of a molecular machine causing chirality manipulation in a controllable and reversible manner.

**7.3.4.3. Chirality Transfer via Ternary Complex.** Recently, Aida and co-workers [85] have created many similar compounds incorporating the molecular scissor as a basis for more elaborate and complex systems. Such systems include a ternary compound, which includes a pyridine-appended dithienylethene derivative as a photochromic module that can again be used to transfer conformational information with UV and visible light as a trigger [85]. Extension of the pivotal ferrocene has also been adopted in reversible self-locking compounds shown in Figure 7.25. In the presence of *trans*-1,2-bispyridine ethylene, the zinc–porphyrin moieties coordinate intramolecularly with the anilines to “lock” the molecule internally [86]. UV light is then used to isomerize to the *cis*-1,2-bispyridine ethylene that is then capable of coordinating to the zinc porphyrin units, “locking” the molecules externally. The process is again shown to be reversible by alternating UV and visible light irradiation. Such discoveries by Aida and co-workers could help to controllably transmit chiral and mechanical information through long molecular distances.

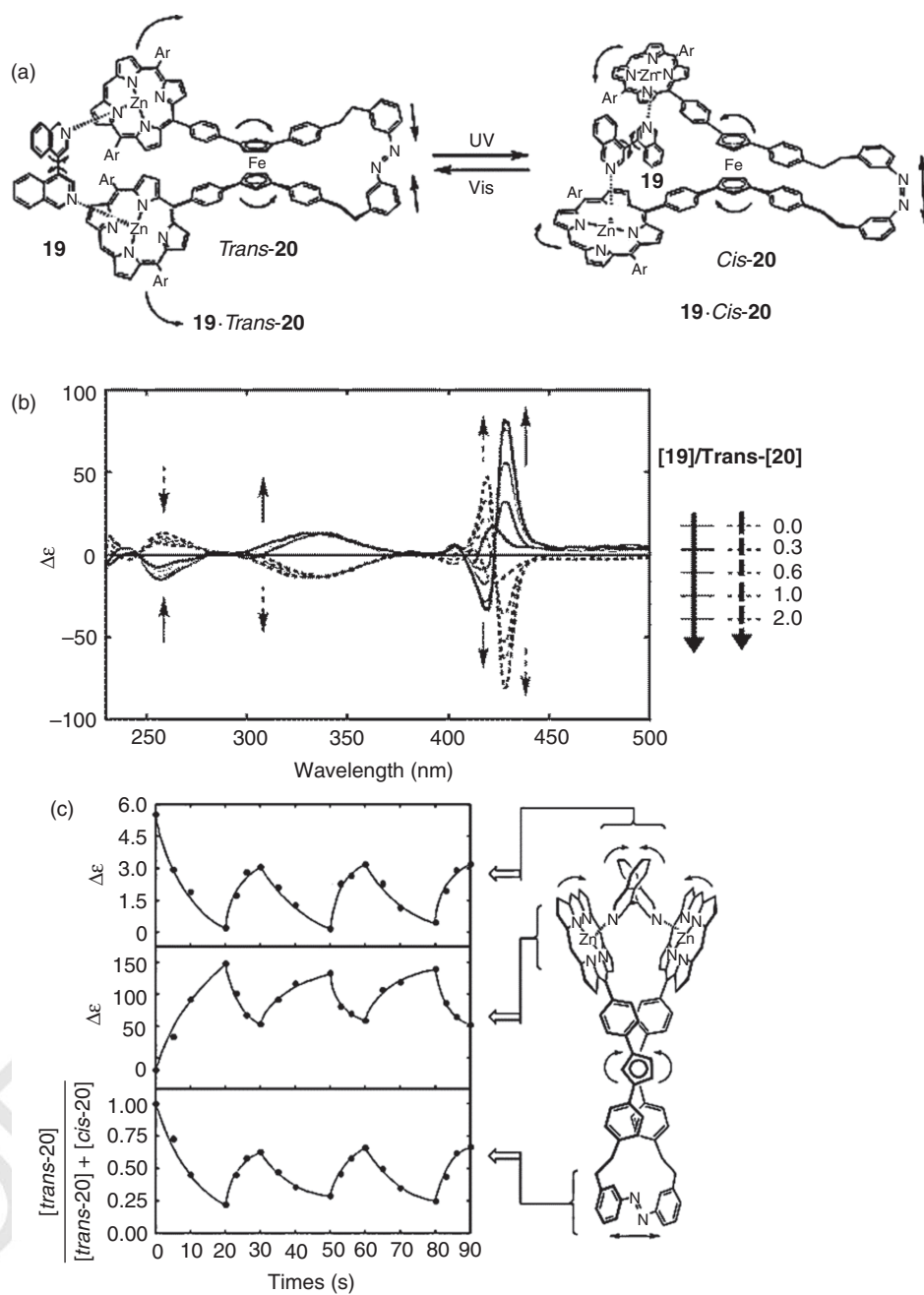


**Figure 7.24.** (a) Photoisomerization of a 1:1 complex of molecular pedal **20** with rotary guest **19** (**19**·**20**). (b) CD spectral changes of **trans-20** upon titration with **19**. (c) CD visualization of the motions of guest-binding molecular pedals **19**·(+)-**20** and **19**·(-)-**20** triggered by light [84]. (Reprinted by permission from Macmillan Publishers Ltd: Copyright 2006.)



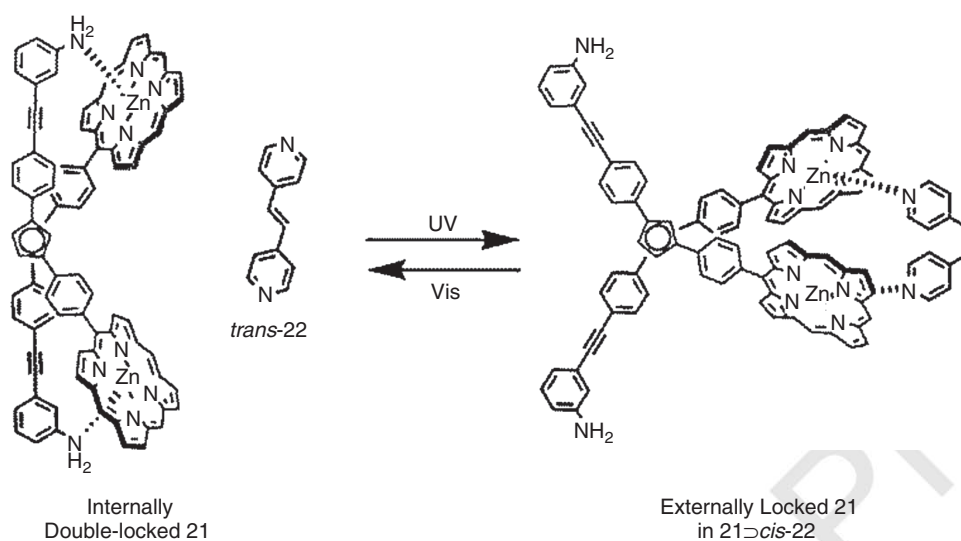


**Figure 7.25.** Structures of internally double-locked **21** and externally locked **21**  $\supset$  *cis*-**22**, and the self-locking operation in response to photochemical isomerization of **22** [86]. (Reproduced by permission of the Royal Society of Chemistry.)

#### 7.4. DYNAMIC STEREOCHEMISTRY MONITORED BY VCD

VCD spectra have been applied to study transition-metal complexes since the pioneering work by Nafie and co-workers [8, 13, 87] VCD spectroscopy was applied to monitoring *in situ* the photoinduced rewind of supramolecular helices in a liquid crystal (Figure 7.26) [11]. A room-temperature liquid crystal, ZLI-1132, was doped with a chiral Cr(III) complex  $\Delta$ -[Cr(acac)<sub>2</sub>(2C12)] (acac = acetylacetonate; 2C12 = 4,4'-didodecyloxyated dibenzoylmethanate). The selective reflection wavelength  $\lambda_c = np$  ( $n$  is the average refractive index,  $p$  is the pitch length of an induced helix) of the nematic phase was determined to be 5.3  $\mu\text{m}$ . At this wavelength, circularly polarized light reflects from or passes through the sample when it has the same or opposite sense of the induced helix, respectively. Under the illumination of UV light (365 nm), the photoracemization of the Cr(III) complex led to the rewind of helices in the chiral nematic phase. In response to this, the VCD spectrum of the system exhibited the transient change.

Figure 7.26 shows the time course of the VCD spectrum when it was recorded every 30 min. The peak at  $1610\text{ cm}^{-1}$  increased its intensity for the initial 1 h. The change reflected the elongation of the pitch maintaining the relation of  $\lambda/\lambda_c > 1$ . The peak underwent a drastic change at 1.5 h: the spectral shape transformed from a Gaussian to a biphasic one, which indicated the relation of  $\lambda/\lambda_c = 1$  was fulfilled at this stage. After 2 h, the peak returned to a Gaussian shape with a negative sign, indicating the relation of  $\lambda/\lambda_c < 1$ . In this way, the observed inversion of the VCD sign is theoretically predicted. Reflecting the further elongation of the helical pitch, the position of a biphasic peak shifted toward the longer wavelength. When the VCD spectrum is regarded as a memory signal for the photoresponsive events in this liquid-crystalline system, it shows high signal-to-noise ratio (S/N) since it changes the sign as well as the intensity. The spectral change conveys the information of time memory because the position of the biphasic shaped peak shifts toward the longer wavelength on continuing irradiation. It

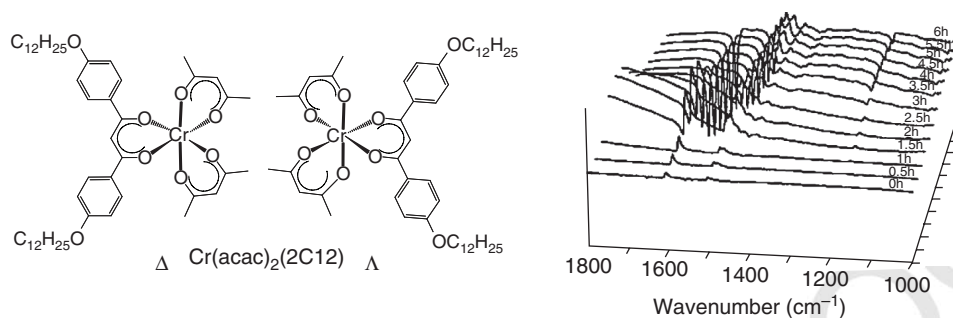


**Figure 7.26.** VCD spectra of a chiral nematic sample of ZLI-1132 doped with 0.538 mol%  $\Delta$ -[Cr(acac)<sub>2</sub>(2C12)] at various times after UV light (365 nm) irradiation [11]. (Reproduced by permission of Taylor and Francis.)

shows extremely stable memory since the racemization process is accompanied by an increase of entropy, thus irreversible.

## 7.5. DYNAMIC STEREOCHEMISTRY MONITORED BY FD CD AND CPE

Fluorescence-detected circular dichroism (FD CD) is a method that can measure the CD response by detection in emission if the chromophore is also fluorescent. This method was originally developed by Tinoco and co-workers [88, 89] and studied intensively more recently by Berova, Nakanishi, and co-workers [90–92]. While conventional CD measures the difference in a sample's absorption of left- and right-circularly polarized light, FD CD measures the difference in fluorescence intensity upon excitation by left- and right-circularly polarized light. Since it is usually true that the excitation spectrum of a fluorophore parallels its absorption, the same circular dichroic information should be able to be extracted from both processes if the artifacts related to undesired fluorescence anisotropy are eliminated by more advanced instrumentation [92]. FD CD has been shown to be more sensitive than absorption CD [90, 93], analogous to the fact that fluorescence spectroscopy is more sensitive than the UV–vis absorption method because fluorescence suffers no background interference from the incident light. Raw FD CD data measured by a JASCO circular dichroism system equipped with FD CD attachment and with the fluorescence detector placed at 90° to the excitation beam (i.e., 90° to the CD detector) have two channels [90]. They represent excitation spectra and correspond to the difference in emission  $\Delta F (F_L - F_R)$  and the total emission  $(F_L + F_R)$  resulting from differential absorption of left- and right-circularly polarized light, respectively. Typically, the data are converted to CD spectra by established methods, which gives a normal CD spectrum if fluorescence polarization is negligible: The FD CD and normal CD of the zinc complex of a chiral tripodal ligand match perfectly.

An adaptation of the FD CD technique can provide a unique and powerful new strategy for sensor applications by using the  $\Delta F$ , that is,  $(F_L - F_R)$ , component of FD CD data directly, without conversion to CD. To distinguish this new approach from traditional FD CD and to avoid confusion, this method was named differential circularly polarized fluorescence excitation (CPE) [17], although no new instrument is required and all of the advantages and nature of FD CD still pertain. This is different from circularly polarized luminescence (CPL) because CPL is the differential spontaneous emission of left- and right-circularly polarized light and reflects the structural properties of the excited

state, while CPE is still an indirect reflection of the structural properties of the ground electronic state. The theoretical basis of CPE is shown in the following equation and can be derived from long-established Eq. (7.1) [90].

$$\Delta F = \frac{\theta \cdot (F_L + F_R) \cdot \ln 10}{33 \cdot 2 \cdot (10^A - 1) \cdot k} \quad (7.1)$$

If  $\Delta A = A_L - A_R \leq 0.1$  and  $\Delta A/A \leq 0.1$ , total emission ( $F_L + F_R$ ) should be proportional to fluorescence induced by nonpolarized light, that is,

$$F_L + F_R = k_2 \cdot F = k_2 \cdot \Phi_F \cdot I^0 \cdot (1 - 10^{-A}), \quad (7.2)$$

Therefore Eq. (7.1) can be simplified as shown in Eq. (7.3), where  $K$  is a constant, which incorporates all other constants and  $\Phi_F$  is the fluorescence quantum yield.

$$\Delta F = \frac{\theta \cdot \Phi_F \cdot I^0 \cdot k_2 \cdot \ln 10}{33 \cdot 2 \cdot 10^A \cdot k} = K \cdot \frac{\theta \cdot \Phi_F \cdot I^0}{10^A} \quad (7.3)$$

Materials with higher ellipticity  $\theta$  and higher fluorescence quantum yield  $\Phi_F$  will lead to an even larger  $\Delta F$ . Substances lacking either fluorescence or CD properties will not be observed. Shown in Figure 7.27 are the CD and CPE ( $\Delta F$ ) responses of a chiral piperidine compound (**23**) to  $\text{Zn}^{2+}$  [17]. Apparently, FDCD and CPE may be used to monitor the chirality switching in such metal complexes.

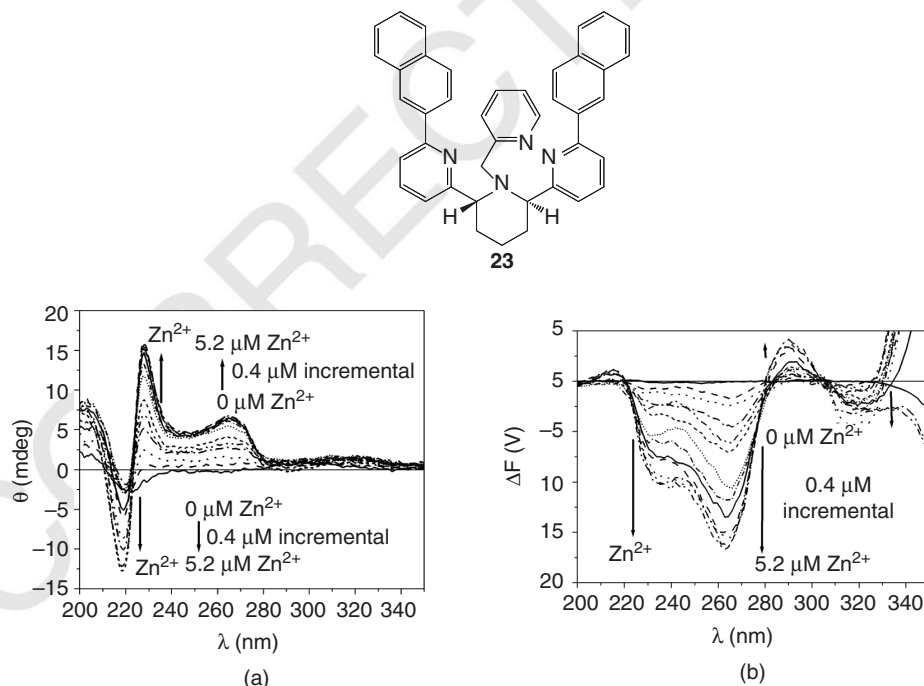


**Figure 7.27.** Spectral responses of  $4.8 \mu\text{M}$  (***R,R***-**23**) to  $0$ – $5.2 \mu\text{M}$   $\text{Zn(II)}$  in acetonitrile. (a) CD. (b) CPE (700V, 81 deg, filter: 360 nm) [17]. (Reproduced by permission of the American Chemical Society.)

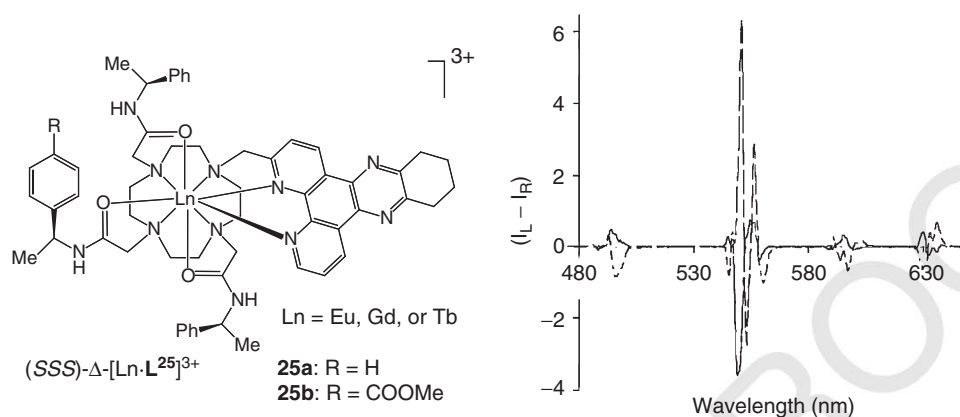


**Figure 7.28.** (Left) CPL spectra for  $(SSS)\text{-}\Delta\text{-[Tb}\cdot\text{L}^{25}\text{]}^{3+}$  (solid curve) and in the presence of BSA (broken curve). (Right) Chiral lanthanide metal–ligand complex used to bind human or bovine serum albumin in “drug site II” [18]. (Reproduced by permission of the Royal Society of Chemistry.)

## 7.6. DYNAMIC STEREOCHEMISTRY MONITORED BY CPL

Circularly polarized luminescence (CPL), the anisotropic emission of circularly polarized light originated from nonpolarized excitation, is the emission analogue to CD. The sign and magnitude of CPL are affected by the degree of helical twist of the complex, the nature of the ligand field, and other factors. In this context, excited Ln(III) ions can be considered as “spherical” emitters and avoid the problems associated with anisotropy that can complicate some chiroptical analyses [94]. CPL reflects the time-averaged local helicity around the lanthanide(III) ion. The Parker group has recently utilized the chiral environment of drug site II of serum albumin to induce helicity inversion in complexes of terbium and europium (III) [18]. It was found that chiral complex  $(S,S,S)\text{-}\Delta\text{-[Tb}\cdot\text{L}^{25}\text{]}^{3+}$  changed helicity to  $(S,S,S)\text{-}\Lambda\text{-[Tb}\cdot\text{L}^{25}\text{]}^{3+}$  upon addition of human or bovine serum albumin. Convincing data was supplied by circularly polarized emission (Figure 7.28). When the  $\Delta$ -isomer is exposed to BSA or HSA, there is an inversion of the sign of emission and 35% reduction of the signal intensity. The authors explain that the emission spectra “are consistent with the inversion of the helicity of the complex in the protein-bound form” [95]. Parallel experiments were run using the  $\Lambda$ -isomer, but no change in emission spectra was found. These results give one of the few immediately biologically relevant examples of a metal-based chiroptical molecular switch. The system could potentially allow protein association to be tracked *in vitro* in real time.

## 7.7. SOLID-STATE METAL-BASED CHIROPTICAL SWITCHES

### 7.7.1. Pressure-based switches

Pressure also has been reported to induce chiroptical responses in chiral metal complexes. In solution, high pressure can provide a powerful solvent effect since dispersive interactions depend strongly on density changes. In the solid state, crystal packing plays an additional role. The effect of pressure on circular CD spectra of the octahedral chiral  $\Lambda$ -,  $\Delta$ -, and  $(\Lambda,\Delta)\text{tris}\{\text{O},\text{O}'\text{-bis}[(+)\text{(S)-2-methylbutyl}]\text{dithiophosphate}\}\text{Cr(III)}$

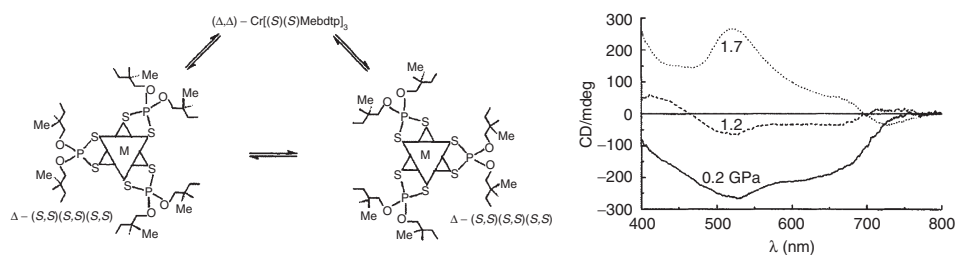


**Figure 7.29.** CD spectra at different pressures of solid  $\Delta$ -tris[O,O'-bis[(+)(S)-2-methylbutyl]dithiophosphate]Cr(III) and proposed  $\Delta$ ,  $\Delta$  conversion mechanism [96]. (Reproduced by permission of Taylor and Francis.)

complexes was studied in the pressure range 0–2.5 GPa (Figure 7.29) [96]. Results on polycrystalline samples dispersed in nujol show a pressure-induced  $\Delta$ -to- $\Delta$  inversion of configuration at the metal center above 1.2 GPa, which was suggested to arise from differential crystal packing in the solid-state structure of the diastomeric complexes. The  $\Delta$ -form is confirmed to be the most favored crystal packing among different ligand conformations of the chiral complex under high pressure. When the applied pressure exceeded 2.5 GPa, the CD band obtained from polycrystalline Nujol samples of chiral  $\Delta$  and  $\Delta$ -tris-[cyclic O,O', 1(*R*), 2(*R*)-dimethylethylene dithiophosphato]chromium (III) complexes inverted from negative to positive, which demonstrated inversion from the  $\Delta$ -form to the  $\Delta$ -form by means of pressure [97, 98]. To minimize artifacts, the spectra were obtained from average data from rotating the diamond anvil cell (DAC) around its optical axis, and the reference spectrum was normalized outside the absorption region of the sample. The cycle was reversible as demonstrated by applying repeating pressure cycles. However, the transition pressure varied and was dependent on the amount of  $\Delta$ -diastereomer present in the sample. Mechanistic explanation of the pressure induced chirality inversion could involve bond breaking or trigonal twisting around the metal center. It would be interesting to see if other solid-state data could be obtained to test the mechanistic hypothesis and exclude artifacts.

### 7.7.2. Temperature-Induced Dynamic Stereochemistry

The compound  $\alpha$ -Ni(H<sub>2</sub>O)<sub>6</sub> · O<sub>4</sub> and its selenate derivative exhibit chirality only in the solid state. The Kuroda group observed a remarkable reversible sign inversion of CD in the  $^3A_{2g} \rightarrow ^3T_{1g}(P)$  Ni(II) *d*–*d* transition at near liquid nitrogen temperatures, although the crystal structure hardly changes from 300 to 100 K (Figure 7.30) [99]. The change in Ni<sup>2+</sup> electronic states at low temperatures might have altered the relative magnitude of the opposite sign first- and second-order rotational strengths.

### 7.7.3. Photo-induced Switching

Switching of molecular chirality under photoirradiation was studied in a cobaloxime complex crystal using CD (Figure 7.31) [100]. The (*S*-alkyl)(*S*-base) crystal was irradiated using two different wavelength bands, one with 439–499 nm covering the LMCT transition and the other with 640–900 nm covering the triplet *d*–*d* transition of Co(III). After irradiation with either wavelength band, the solid was dissolved in methanol and the changes in its CD spectrum were recorded. Excitation of the *d*–*d* transition of the Co(III) ion appeared to be much more effective in inducing the chirality change than



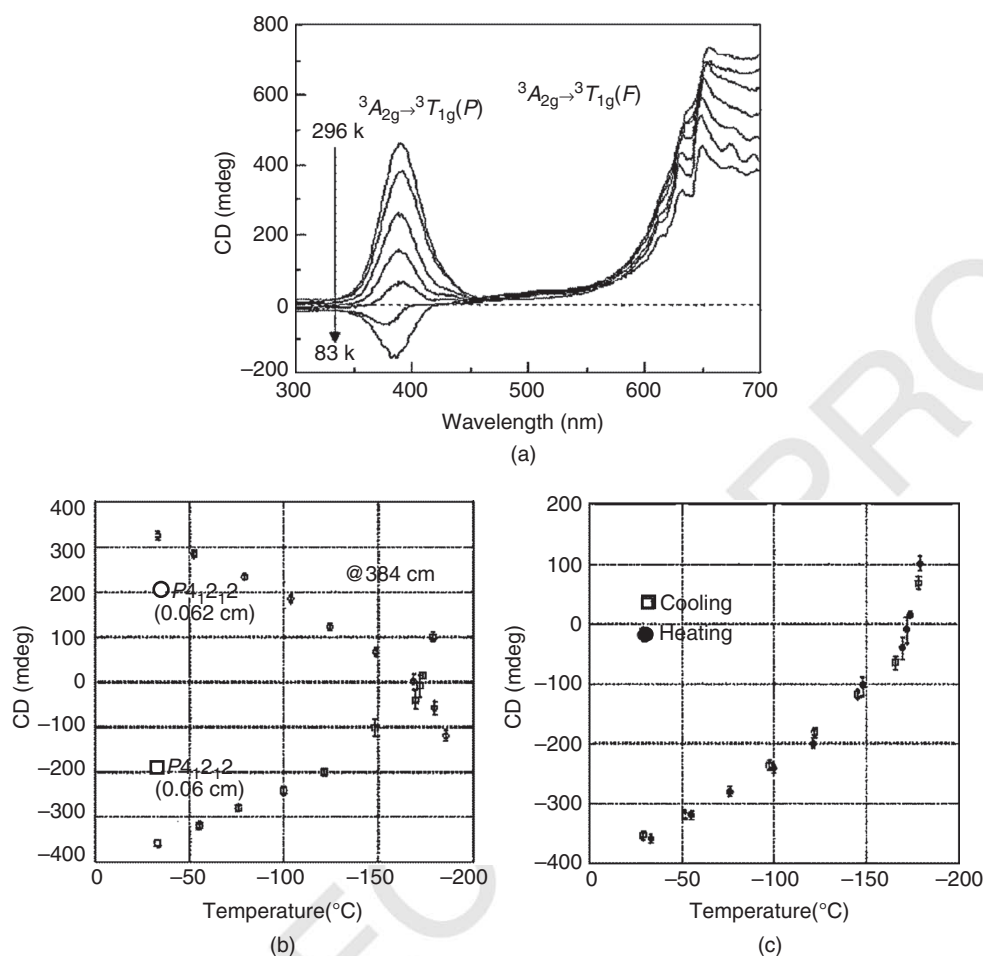


**Figure 7.30.** (a) Observed CD spectra of the same  $\alpha$ -Ni(H<sub>2</sub>O)<sub>6</sub> · SO<sub>4</sub> single crystal (P<sub>4</sub><sub>3</sub>2<sub>1</sub>2, 0.062-mm thickness) at different temperatures. (b) CD signal at 384 nm plotted against temperature for the enantiomorphous  $\alpha$ -Ni(H<sub>2</sub>O)<sub>6</sub> · SO<sub>4</sub> single crystals. ○: P<sub>4</sub><sub>3</sub>2<sub>1</sub>2 (0.62 mm thickness); □: P<sub>4</sub><sub>1</sub>2<sub>1</sub>2 (0.60 mm thickness). (c) Temperature dependence of the CD values of P<sub>4</sub><sub>1</sub>2<sub>1</sub>2 crystal on cooling (□) and on heating (●) [99]. (Reproduced by permission of Elsevier.)

excitation of the ligand–metal charge transfer band, although the latter is more effective in breaking the Co–C bond that initiates the chirality switching. The chirality change versus irradiation time showed a step-like behavior suggesting that chirality switching of molecules occurred in correlation with their nearest neighbors.

The same group made direct observation of a photoinduced chirality change or switching in the alkyl ligand of the cobaloxime complex in the hydrated and nonhydrated crystals of the cobaloxime complex by direct CD measurements in the solid phase in Nujol-mull and KBr pellets [101]. The CD spectra of the two crystal forms showed clear differences. Additional CD spectral peaks in the spectra of the nonhydrated crystals seemed to arise from exciton splitting of the charge-transfer band. Photoirradiation induced chirality change or switching in the alkyl part of the molecule, but not in the crystal structure. The CD spectra well reflect such behavior.



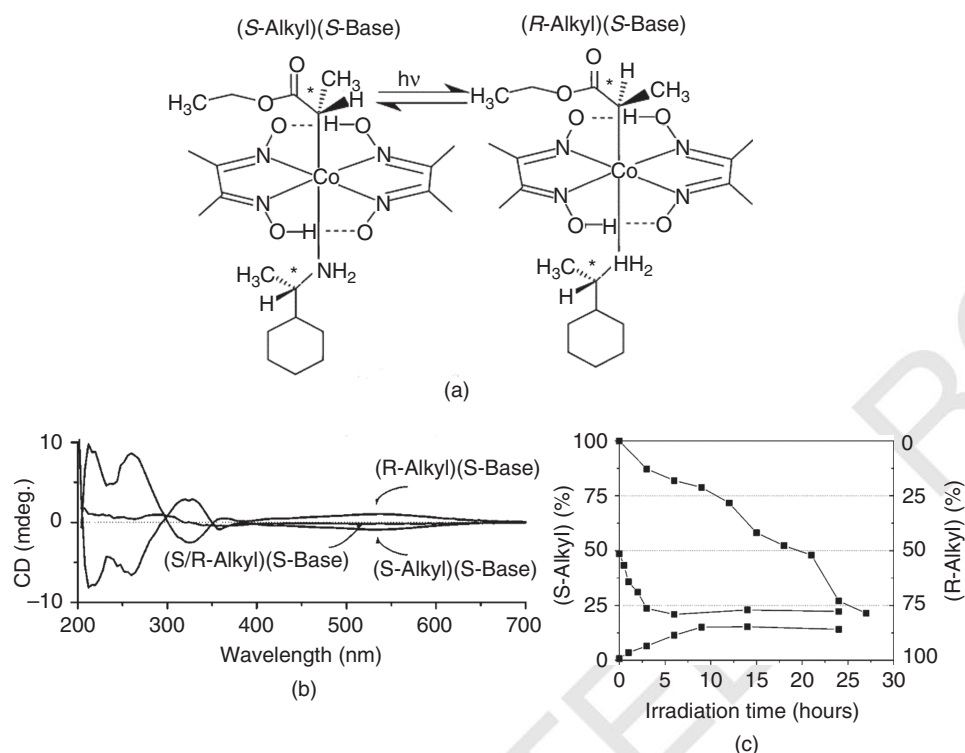


**Figure 7.31.** (a) Molecular structures of a pair of diastereomers of cobaloxime complex that can be converted to each other by photoisomerization. (b) CD spectra of (S-alkyl)(S-base), (R-alkyl)(S-base), (S/R-alkyl)(S-base) cobaloxime complexes in 1-mM methanol solution. (c) Time variation of photoinduced chirality change in the cobaloxime complex crystals of (S-alkyl)(S-base), (R-alkyl)(S-base), and (S/R-alkyl)(S-base) under constant irradiation of light with wavelength of 640–900 nm [100]. (Reproduced by permission of the American Institute of Physics.)

## 7.8. CONCLUSIONS

The future of metal-based chiroptical switches is bright, given the high degree of control available, a multitude of triggering mechanisms, and powerful chiroptical spectroscopy tools available for analysis. With the large number of recently discovered systems, these compounds and materials derived from them could potentially be used for applications including optical displays, complex molecular electronics, chiral resolution, and catalysis.

The Pfeiffer effect and metal ion templated synthesis provided early chemistry relevant to more recently developed metal-based chiroptical switches. Environment-responsive switches have been developed using a large variety of metals and ligands triggered by pressure, counterion alteration, light, and solvent changes. Redox triggered switches have been explored primarily using a tripodal ligand motif. Diazobenzene-ferrocene systems were designed to reliably switch the conformations of a set of “molecular scissors,” which were then used in an array of interesting and complex supramolecular machines. Polymer systems have been explored illustrated by the use of metal dopants to cause chiroptical changes in oligothiophene polymers. The studies in this area have

provided much stimulating new chemistry and exemplify the power of modern molecular design and solution characterization techniques. There is no doubt that there are many more opportunities to develop even more imaginative systems. Many applications for these materials have been discussed, especially in the areas of electronics and sensors, and several of the available systems are poised to make a genuine contribution.

Although early phenomena were studied by ORD, electronic circular dichroism experiments were used in nearly all experiments to analyze the conformational changes of the chiral compounds. Although other analytical techniques such as NMR are used to study these systems, it is readily apparent that CD experiments provide accurate and dependable read-out for chiral metal-based switches. The exciton chirality method has been particularly useful as a result of the fact that it gives a sizable and interpretable signal. Indeed, few other spectroscopic measurements give a direct report of three-dimensional shape as exciton chirality does for the orientation of chromophoric units. However, care should be taken in the assignment of CD data as arising from exciton coupling.

Newer chiroptical spectroscopic methods are beginning to contribute to this field. The first reports of systems employing NIR-CD, which offers low-energy measurement, have appeared. FDCD can provide very sensitive detection if precautions are taken to avoid artifacts. FDCD or CPE may offer more specific information since it may arise from a subset of transitions compared to CD. VCD offers the possibility to probe vibrational phenomena as illustrated in studies of memory in liquid crystalline switches. All of these newer methods are ripe for further development in chiroptical switch detection strategies. It is also high time for computational methods coupled with chiroptical spectroscopy to play a greater role in not only characterization but also design of these systems.

Most metal-based chiroptical switches reported to date were studied in solution, but many applications of chiroptical molecular switches involve the solid phase where chiroptical spectra are more difficult to interpret. Fortunately, the development of solid phase characterization tools and accompanying theory is progressing. In this regard, computation has resulted in renewed interest in ORD and other classic methods due to the possibility of making structural conclusions by matching experiment with theory.

## ACKNOWLEDGMENTS

We are grateful to the National Science Foundation (CHE-0848234) for generous support of our work in this area. ZD thanks Research Corporation for Science Advancement and the donors of the American Chemical Society Petroleum Research Fund for support of this work.

## REFERENCES

1. L. Fabbrizzi, A. Poggi, *Transition Metals in Supramolecular Chemistry*, Kluwer Academic Publishers, Dordrecht, **1994**.
2. B. Champin, P. Mobian, J. P. Sauvage, *Chem. Soc. Rev.* **2007**, 36, 358–366.
3. H. Amouri, M. Gruselle, *Chirality in Transition Metal Chemistry: Molecules, Supramolecular Assemblies and Materials*, Wiley, Chichester, **2008**.
4. H. Miyake, H. Tsukube, *Supramol. Chem.* **2005**, 17, 53–59.
5. M. Elhabiri, A. M. Albrecht-Gary, *Coord. Chem. Rev.* **2008**, 252, 1079–1092.

6. K. Nakanishi, N. Berova, R. Woody, *Circular Dichroism: Principles and Applications*, Wiley-VCH, New York, **2000**
7. S. Allenmark, J. Gawronski, *Chirality* **2008**, *20*, 606–608.
8. P. L. Polavarapu, L. A. Nafie, S. A. Benner, T. H. Morton, *J. Am. Chem. Soc.* **1981**, *103*, 5349–5359.
9. L. A. Nafie, *J. Mol. Spectrosc.* **1995**, *347*, 83–100.
10. T. B. Freedman, X. Cao, R. K. Dukor, L. A. Nafie, *Chirality* **2003**, *15*, 743–758.
11. T. Taniguchi, K. Monde, S.-I. Nishimura, J. Yoshida, H. Sato, A. Yamagishi, *Mol. Cryst. Liq. Cryst.* **2006**, *460*, 107–116.
12. H. Sato, D. Shirotani, K. Yamanari, S. Kaizaki, *Inorg. Chem.* **2010**, *49*, 356–358.
13. D. A. Young, E. D. Lipp, L. A. Nafie, *J. Am. Chem. Soc.* **1985**, *107*, 6205–6213.
14. S. Abbate, E. Castiglioni, F. Gangemi, R. Gangemi, G. Longhi, *Chirality* **2009**, *21*, E242–E252.
15. C. Guo, R. D. Shah, R. K. Dukor, X. Cao, T. B. Freedman, L. A. Nafie, *Chirality* **2005**, *59*, 1114–1124.
16. N. Berova, L. Di Bari, G. Pescitelli, *Chem. Soc. Rev.* **2007**, *36*, 914–931.
17. Z. Dai, G. Proni, D. Mancheno, S. Karimi, N. Berova, J. W. Canary, *J. Am. Chem. Soc.* **2004**, *126*, 11760–11761.
18. C. P. Montgomery, E. J. New, D. Parker, R. D. Peacock, *Chem Commun.* **2008**, 4261–4263.
19. T. Harada, H. Hayakawa, R. Kuroda, *Rev. Sci. Instrum.* **2008**, *79*, 073103.
20. A. Werner, *Ann.* **1912**, *386*, 1.
21. D. B. Shapiro, R. A. Goldbeck, D. Che, R. M. Esquerra, S. J. Paquette, D. S. Kliger, *Biophys. J.* **2005**, *68*, 326–334.
22. M. Krykunov, M. D. Kundrat, J. Autschbach, *J. Chem. Phys.* **2006**, *125*, 194110–194113.
23. H. Yoneda, Y. Nakashima, U. Sakaguchi, *Chem. Lett.* **1973**, 1343–1346.
24. D. W. Urry, H. Eyrin, *J. Am. Chem. Soc.* **1964**, *86*, 4574–4580.
25. W. T. Shearer, R. K. Brown, *J. Biol. Chem.* **1966**, *241*, 2665–2671.
26. E. Cerasoli, B. K. Sharpe, D. N. Woolfson, *J. Am. Chem. Soc.* **2005**, *127*, 15008–15009.
27. K. Pagel, T. Vagt, T. Kohajda, B. Koksche, *Org. Biomol. Chem.* **2005**, *3*, 2500–2502.
28. I. Otsuka, R. Sakai, T. Satoh, R. Kakuchi, H. Kaga, T. Kakuchi, *J. Polymer Sci. A: Polymer Chem.* **2005**, *43*, 5855–5863.
29. T. Sanji, Y. Sato, N. Kato, M. Tanaka, *Macromolecules* **2007**, *40*, 4747–4749.
30. H. Goto, E. Yashima, *J. Am. Chem. Soc.* **2002**, *124*, 7943–7949.
31. O. Henze, W. J. Feast, F. Gardebien, P. Jonkheijm, R. Lazzaroni, P. Leclère, E. W. Meijer, A. P. H. J. Schenning, *J. Am. Chem. Soc.* **2006**, *128*, 5923–5929.
32. S. Haraguchi, M. Numata, C. Li, Y. Nakano, M. Fujiki, S. Shinkai, *Chem. Lett.* **2009**, *38*, 254–255.
33. L. A. P. Kane-Maguire, G. G. Wallace, *Chem. Soc. Rev.* **2010**, *39*, 2545–2576.
34. M. Funahashi, N. Tamaoki, *Chem. Mater.* **2007**, *19*, 608–617.
35. P. Pfeiffer, K. Quehl, *Ber.* **1931**, *64*, 2667.
36. H. G. Brittain, *Polyhedron* **1984**, *3*, 1087.
37. G. A. Hembury, V. V. Borovkov, Y. Inoue, *Chem. Rev.* **2008**, *108*, 1–73.
38. N. Wei, N. N. Murthy, K. D. Karlin, *Inorg. Chem.* **1994**, *33*, 6093–6100.
39. J. W. Canary, A. E. Holmes, J. Liu, *Enantiomer* **2001**, *6*, 181–188.
40. H. Ishii, Y. Chen, R. A. Miller, S. Karady, K. Nakanishi, N. Berova, *Chirality* **2005**, *17*, 305–315.
41. N. Berova, G. Pescitelli, A. G. Petrovic, G. Proni, *Chem. Commun.* **2009**, 5958–5980.

42. X. Li, B. Borhan, *J. Am. Chem. Soc.* **2008**, *130*, 16126–16127.
43. V. V. Borovkov, J. M. Lintuluoto, Y. Inoue, *Org. Lett.* **2000**, *2*, 1565–1568.
44. V. V. Borovkov, G. A. Hembury, Y. Inoue, *Acc. Chem. Res.* **2004**, *37*, 449–459.
45. S. Nieto, V. M. Lynch, E. V. Anslyn, H. Kim, J. Chin, *Org. Lett.* **2008**, *10*, 5167–5170.
46. S. Nieto, V. M. Lynch, E. V. Anslyn, H. Kim, J. Chin, *J. Am. Chem. Soc.* **2008**, *130*, 9232–9233.
47. S. Yano, M. Nakagoshi, A. Teratani, M. Kato, T. Onaka, M. Iida, T. Tanase, Y. Yamamoto, H. Uekusa, Y. Ohashi, *Inorg. Chem.* **1997**, *36*, 4187–4194.
48. H. Miyake, K. Yoshida, H. Sugimoto, H. Tsukube, *J. Am. Chem. Soc.* **2004**, *126*, 6524–6525.
49. H. Miyake, H. Sugimoto, H. Tamiaki, H. Tsukube, *Chem. Commun.* **2005**, *34*, 4291–4293.
50. H. Miyake, M. Hikita, M. Itazaki, H. Nakazawa, H. Sugimoto, H. Tsukube, *Chem.-Eur. J.* **2008**, *14*, 5393–5396.
51. H. Miyake, H. Kamon, I. Miyahara, H. Sugimoto, H. Tsukube, *J. Am. Chem. Soc.* **2008**, *130*, 792–793.
52. J. Gregolinski, J. Lisowski, *Angew. Chem. Intl. Ed.* **2006**, *45*, 6122–6126.
53. J. Gregolinski, T. Lis, M. Cyganik, J. Lisowski, *Inorg. Chem.* **2008**, *47*, 11527–11534.
54. J. Gregolinski, K. Slepokura, J. Lisowski, *Inorg. Chem.* **2007**, *46*, 7923–7934.
55. J. Gregolinski, P. Starynowicz, K. T. Hua, J. L. Lunkley, G. Muller, J. Lisowski, *J. Am. Chem. Soc.* **2008**, *130*, 17761–17773.
56. M. Lama, O. Mamula, G. S. Kottas, L. De Cola, H. Stoeckli-Evans, S. Shova, *Inorg. Chem.* **2008**, *47*, 8000–8015.
57. M. Hutin, J. Nitschke, *Chem. Commun.* **2006**, 1724–1726.
58. L. Zelikovich, J. Libman, A. Shanzer, *Nature* **1995**, *374*, 790–792.
59. J. W. Canary, C. S. Allen, J. M. Castagnetto, Y. H. Wang, *J. Am. Chem. Soc.* **1995**, *117*, 8484–8485.
60. J. W. Canary, *Chem. Soc. Rev.* **2009**, *38*, 747–756.
61. J. W. Canary, C. S. Allen, J. M. Castagnetto, Y. H. Chiu, P. J. Toscano, Y. H. Wang, *Inorg. Chem.* **1998**, *37*, 6255–6262.
62. X. D. Xu, K. J. Maresca, D. Das, S. Zahn, J. Zubieta, J. W. Canary, *Chem. Eur. J.* **2002**, *8*, 5679–5683.
63. J. M. Castagnetto, X. D. Xu, N. D. Berova, J. W. Canary, *Chirality* **1997**, *9*, 616–622.
64. S. Zahn, J. W. Canary, *Angew. Chem. Intl. Ed.* **1998**, *37*, 305–307.
65. S. Zahn, J. W. Canary, *J. Am. Chem. Soc.* **2002**, *124*, 9204–9211.
66. J. Zhang, K. Siu, C. H. Lin, J. W. Canary, *New J. Chem.* **2005**, *29*, 1147–1151.
67. S. Zahn, G. Proni, G. P. Spada, J. W. Canary, *Chem. Eur. J.* **2001**, *7*, 88–93.
68. J. Zhang, J. W. Canary, *Org. Lett.* **2006**, *8*, 3907–3910.
69. A. E. Holmes, S. Zahn, J. W. Canary, *Chirality* **2002**, *14*, 471–477.
70. S. Zahn, J. W. Canary, *Org. Lett.* **1999**, *1*, 861–864.
71. S. Zahn, J. W. Canary, *Science* **2000**, *288*, 1404–1407.
72. S. Zahn, D. Das, J. W. Canary, *Inorg. Chem.* **2006**, *45*, 6056–6063.
73. H. S. Barcena, A. E. Holmes, J. W. Canary, *Org. Lett.* **2003**, 709–711.
74. A. Company, M. Guell, D. Popa, J. Benet-Buchholz, T. Parella, X. Fontrodona, A. Llobet, M. Sola, X. Ribas, J. M. Luis, M. Costas, *Inorg. Chem.* **2006**, *45*, 9643–9645.
75. S. Yamaguchi, T. Katoh, H. Shinokubo, A. Osuka, *J. Am. Chem. Soc.* **2008**, *130*, 14440–14441.
76. A. E. Holmes, D. Das, J. W. Canary, *J. Am. Chem. Soc.* **2007**, *129*, 1506–1507.

77. G. Pognon, C. Boudon, K. J. Schenk, M. Bonin, B. Bach, J. Weiss, *J. Am. Chem. Soc.* **2006**, *128*, 3488–3489.
78. D. Li, Z. Y. Wang, D. Ma, *Chem. Commun.* **2009**, 1529–1531.
79. Z. Y. Wang, E. K. Todd, X. S. Meng, J. P. Gao, *J. Am. Chem. Soc.* **2005**, *127*, 11552–11553.
80. J. Zheng, W. Qiao, X. Wan, J. P. Gao, Z. Y. Wang, *Chem. Mater.* **2008**, *20*, 6163–6168.
81. J. Deng, N. H. Song, W. Liu, Q. F. Zhou, Z. Y. Wang, *ChemPhysChem* **2008**, *9*, 1265–1269.
82. K. Tashiro, K. Konishi, T. Aida, *J. Am. Chem. Soc.* **2000**, *122*, 7921–7926.
83. T. Muraoka, K. Kinbara, Y. Kobayashi, T. Aida, *J. Am. Chem. Soc.* **2003**, *125*, 5612–5613.
84. T. Muraoka, K. Kinbara, T. Aida, *Nature* **2006**, *440*, 512–515.
85. H. Kai, S. Nara, K. Kinbara, T. Aida, *J. Am. Chem. Soc.* **2008**, *130*, 6725–6726.
86. K. Kinbara, T. Muraoka, T. Aida, *Org. Biomol. Chem.* **2008**, *6*, 1871–1876.
87. Y. He, X. Cao, L. A. Nafie, T. B. Freedman, *J. Am. Chem. Soc.* **2001**, *123*, 11320–11321.
88. D. H. Turner, I. J. Tinoco, M. Maestre, *J. Am. Chem. Soc.* **1974**, *96*, 4340–4342.
89. I. J. Tinoco, D. H. Turner, *J. Am. Chem. Soc.* **1976**, *98*, 6453–6456.
90. J.-G. Dong, A. Wada, T. Takakuwa, K. Nakanishi, N. Berova, *J. Am. Chem. Soc.* **1997**, *119*, 12024–12025.
91. T. Nehira, C. A. Parish, S. Jockusch, N. J. Turro, K. Nakanishi, N. Berova, *J. Am. Chem. Soc.* **1999**, *121*, 8681–8691.
92. T. Nehira, K. Tanaka, T. Takakuwa, C. Ohshima, H. Masago, G. Pescitelli, A. Wada, N. Berova, *Appl. Spectr.* **2005**, *59*, 121–125.
93. L. Geng, L. B. McGown, *Anal. Chem.* **1992**, *64*, 68–74.
94. J. L. Lunkley, D. Shirotani, Y. Yamanari, S. Kaizaki, G. Muller, *J. Am. Chem. Soc.* **2008**, *130*, 13814–13815.
95. R. A. Poole, C. P. Montgomery, E. J. New, A. Congreve, D. Parker, M. Botta, *Org. Biomol. Chem.* **2007**, *5*, 2055–2062.
96. M. Benedetti, P. Biscarini, A. Brillante, *High Pressure Res.* **2000**, *18*, 285–289.
97. M. Benedetti, P. Biscarini, A. Brillante, E. Castiglioni, *Enantiomer* **1999**, *4*, 63–66.
98. M. Benedetti, P. Biscarini, A. Brillante, *Physica B* **1999**, *265*, 203–207.
99. T. Harada, T. Sato, R. Kuroda, *Chem. Phys. Lett.* **2008**, *456*, 268–271.
100. K. Ikeda, W. Liu, Y. R. Shen, H. Uekusa, Y. Ohashi, S. Koshihara, *J. Chem. Phys.* **2005**, *122*, 141103.
101. K. Ikeda, W. Liu, Y. R. Shen, H. Uekusa, Y. Ohashi, S. Koshihara, *Chem. Phys. Lett.* **2006**, *422*, 267–270.

UNCORRECTED PROOFS



**Queries in Chapter 7**

- Q1. We have shortened the running head since it exceeds page width. Please confirm if it is fine.
- Q2. Please confirm if this volume is ok, or this treatise (i.e., vols 1 & 2)?